Advances in Colloid and Interface Science 267 (2019) 26–46

Contents lists available at ScienceDirect

Advances in Colloid and Interface Science

journal homepage: www.elsevier.com/locate/cis

Historical perspective

Core-shell nanomaterials: Applications in energy storage and conversion

Hao-peng Feng [a,b], Lin Tang [a,b,*], Guang-ming Zeng [a,b,*], Yaoyu Zhou [c], Yao-cheng Deng [c], Xiaoya Ren [a,b], Biao Song [a,b], Chao Liang [a,b], Meng-yun Wei [a,b,d], Jiang-fang Yu [a,b]

[a] College of Environmental Science and Engineering, Hunan University, Changsha 410082, China
[b] Key Laboratory of Environmental Biology and Pollution Control (Hunan University), Ministry of Education, Changsha 410082, Hunan, China
[c] College of Resources and Environment, Hunan Agricultural University, Changsha 410128, China
[d] Hunan Province Cooperative Innovation Center for the Construction & Development of Dongting Lake Ecological Economic Zone, Changde 415000, China

ARTICLE INFO

Article history:
27 January 2019
Available online 06 March 2019

Keywords:
Core-shell
Electrochemistry
Energy storage
Energy conversion

ABSTRACT

Materials with core-shell structures have attracted increasing attention in recent years due to their unique properties and wide applications in energy storage and conversion systems. Through reasonable adjustments of their shells and cores, various types of core-shell structured materials can be fabricated with favorable properties that play significant roles in energy storage and conversion processes. The core-shell material can provide an effective solution to the current energy crisis. Various synthetic strategies used to fabricate core-shell materials, including the atomic layer deposition, chemical vapor deposition and solvothermal method, are briefly mentioned here. A state-of-the -art review of their applications in energy storage and conversion is summarized. The involved energy storage includes supercapacitors, li-ions batteries and hydrogen storage, and the corresponding energy conversion technologies contain quantum dot solar cells, dye-sensitized solar cells, silicon/organic solar cells and fuel cells. In addition, the correlation between the core-shell structures and their performance in energy storage and conversion is introduced, and this finding can provide guidance in designing original core-shell structures with advanced properties.

Contents

Abbreviations: AC, activated carbon; CNTs, carbon nanotubes; CNFs, carbon nanofibers; CPs, conducting polymers; DSSCs, dye-sensitized solar cells; EDLC, electrochemical double layer capacitors; FCs, Fuel cell; FF, the fill factor; HPC, hierarchically porous carbon; IMPS, intensity-modulated photocurrent; LIBs, rechargeable lithium ion batteries; LSPs, localized surface plasmons; LTMO, lithium transition metal oxides; MC, mesoporous carbon; MCMB, mesocarbon microbead; MOFs, metal organic frameworks; OMC, ordered mesoporous carbon; ORR, oxygen reduction reaction; PANI, polyaniline; PCE, power conversion efficiencies; PPy, polypyrrol; PTh, polythiophene; QD-SSCs, Quantum dot-sensitized solar cells; RCFs, derived from rami; η, conversion efficiency; J_{sc}, the short-circuit current density; V_{oc}, the open-circuit voltage; E_g, tunable bandgap energy.

* Corresponding authors.
E-mail addresses: tanglin@hnu.edu.cn (L. Tang), zgming@hnu.edu.cn (G. Zeng).

https://doi.org/10.1016/j.cis.2019.03.001
0001-8686/

1. Introduction

The developments and innovations in nanotechnology and nanoscience have opened numerous opportunities in various fields, such as energy storage [1,2], energy conversion [3,4], nanoelectronics [5–7], nanocatalysis [8–11], integrated catalysis [12], and so on [13–21], due to the pretty unique properties of nanomaterials compared to those bulk materials. In the early stages, single component nanomaterials were studied extensively, and numerous superior properties have been proven, including tunable optical properties, ease of processing, higher ratio of surface atoms, and excellent catalytic performance. With the rapid development of characterization and synthesis techniques, researchers have found that much better properties could be gained by combining multicomponent nanomaterials, and the diversities in their structure and composition could enrich their applications in various fields. Therefore, core-shell structured nanomaterials have become one of the most popular research topics in recent years. Traditionally, composite nanomaterials composed of inner material (core) and outer layer material (shell) are broadly defined as core-shell nanoparticles (the notation of "@" represents the core-shell structure, core@shell).

Among all multicomponent nanomaterials, core-shell structured nanomaterials have attracted increasing concern due to their outstanding properties, which include the following. (i) The ligand effect is dominated by the adsorption capacity of the material due to the existence of diverse atomic groups on its surface. (ii) The ensemble effect contains the interconnections between the shell and core due to changes in the charge transfer between the components influenced by atomic vicinity, thereby affecting the band-structures. (iii) The structure effect is caused by the 3D structural constraints, resulting in the difference in surface atomic activity. Due to the unique physical and chemical properties, core-shell structured nanomaterials have been widely used in energy storage and conversion. For instance, coating noble metal or metal oxides, as a monoatomic layer on the surface of non-noble metal-based nanocomposites (*e.g.*, Co, Fe or Ni), can produce cost effective and atomic economy core-shell structured nanomaterials with superior energy storage capacity and conversion efficiency. Rapid development of technology over the past few decades has enabled researchers to consider traditional energy storage and conversion from a new perspective [22–26]. Nanoparticles containing precious metals (usually as catalytic or active components) can particularly serve as catalysts on the electrode of storage devices. They can now be controlled to regulate their shapes, crystal facets, structure and composition [27–31]. Such controllability of material structure enables researchers to develop new strategies for applications in economical, sustainable and green chemical industry, which is now considered to be one of the most promising yet challenging fields in chemistry [32–36].

Traditionally, due to the difference in arrangements and compositions of core and shell materials, core-shell structured nanomaterials could be divided into several classes, such as organic/organic, organic/inorganic type, *etc* [37]. Currently, along with the increasing interest for nanocomposites with specific functions or improved properties, core-shell structured nanomaterials have attracted more attention because of their multi-functional compositions and structures [38,39], where the synergistic effect between the shells and cores could exist along with the newly generated performance [40–43]. The application of core-shell structured nanomaterials in photo-voltaic cells exhibits remarkable advantages to improve the cost/efficiency ratio by decreasing the probability of charge recombination and enhancing effective optical path. Such useful, unique and tailorable properties provide core-shell structured nanomaterials with significant potential as emerging nanocomposites for energy storage and conversion (Fig. 1).

Researchers in the field of energy conversion and storage are faced with the daunting task of developing low-cost, environmentally benign systems with large energy conversion and storage efficiency. This goal can be relieved by developing nanocomposites with core-shell structural possessing potential advantages. For example, the shell supported by the core guarantees the specific surface architecture depending on the porosity, surface area, *etc*., leading to superior energy storage and conversion performance. Meanwhile, the synergistic interactions between the core and shell allow for higher energy storage capacity and conversion efficiency. The prepared carbon-supported Pd@Co core-shell structured nanoparticles by Wang et al. were applied and exhibited superior performance for the oxygen reduction reaction [44]. Similarly, Hong et al. used Co_3O_4@CoNi-sulfides nanowire arrays as the electrode material for supercapacitors, which displayed excellent electrochemical performance [45]. It is an effective method of covering transition metals surfaces with a monolayer noble-metals shell (*e.g.*, Co@Pt, Fe@Pt) to reduce the content of precious metals in the energy storage and conversion systems. This process can enhance oxygen adsorption energy, thereby improving electrode stability and activity [46,47].

Recently, Du et al. prepared Au nanoparticles surrounded by a film of TiO_2. The core-shell structured nanomaterials were used as the photoanodes for solar cells and showed significantly enhanced efficiency in power conversion systems [48]. The improved conversion capability of the photoanodes materials was principally due to the

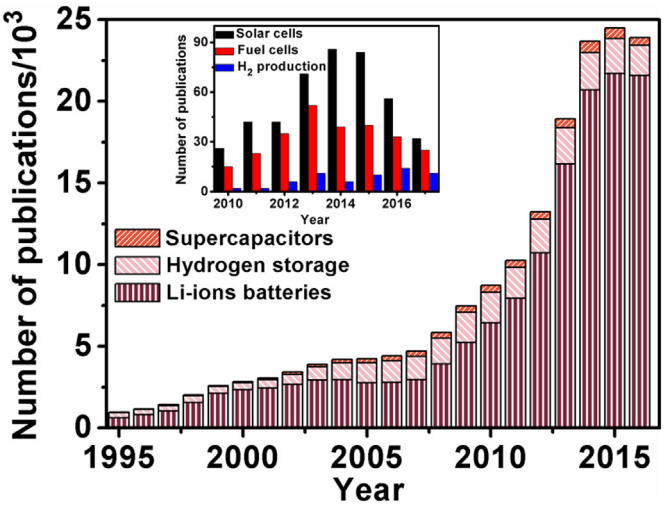

Fig. 1. Trends in the number of publications on core-shell structured materials for supercapacitor, lithium ion battery, and hydrogen storage. Inset: trends in the number of publications on core-shell structured nanomaterials for energy conversion in last five years, including solar cells, Fuel cells, and hydrogen production (data obtained from Web of Science on Oct 30, 2017).

existence of the TiO_2 shell, which contains more active sites and is easier to be electronically activated through the Au core. The lattice strain has also been demonstrated to be beneficial in improving the catalytic activity of core-shell structured nanomaterials. Au@Co core-shell structured nanomaterials prepared by Li et al. [49] and Xu et al. [50] exhibited superior catalytic activity for hydrogen evolution reaction. In another example, Ag nanowires@TiO_2 core-shell structured nanomaterials showed excellent performance. They showed high power conversion efficiency, which was superior to single component nanomaterials in the energy conversion systems, such as solar cells [51]. The power conversion efficiency for solar cells is improved by using core-shell structured nanomaterials as electrode materials.

Overall, various core-shell structured nanomaterials with different morphologies (nanotube, spherical, *etc.*), structures (hollow, yolk-shell, *etc.*), compositions (inorganic, organic, *etc.*), synthetic methods (deposition-precipitation, chemical synthesis, *etc.*), and their energy storage and conversion applications are discussed. Their involvements in energy storage systems (*e.g.*, supercapacitors, li-ion batteries, and hydrogen storage) are reviewed. Energy conversion systems, for instance, fuel cells, solar cells, and photocatalytic H_2 production based on core-shell structured nanomaterials, are then discussed.

2. Core-shell structured nanomaterials applied to energy storage

2.1. Core-shell structured nanomaterials for supercapacitors

Supercapacitors are typical energy storage devices including electrochemical double layer capacitors (EDLCs), pseudocapacitors and asymmetric capacitors. They are considered to be the most potential candidates for effective energy storage due to their long life expectancy, high power density, high efficiency and safety. The energy density of supercapacitors is usually hundreds of times greater than that of traditional electrolytic capacitors. EDLCs based on carbon materials have attracted much attention due to its high power density and long cycling life [52,53], which is attributed to the fact that carbon materials have good electronic conductivity, high chemical stability, and large specific surface areas [54]. Various carbon materials, such as mesoporous carbon (MC), ordered mesoporous carbon (OMC), carbon nanotubes (CNTs), activated carbon (AC), carbide-derived carbon, graphene and hierarchically porous carbon (HPC), *etc*., have been synthesized and researched for supercapacitors.

However, it is practically difficult to obtain a single nanostructured electrode material simultaneously with fast charging/discharging rate, high energy density, and long cycle performance owing to some inherent limitations of individual composition. For instance, carbon materials have excellent cyclical stability and high rate capability while faced with low specific capacitance. To solve these obstacles, various applicable strategies have been proposed. For example, some researchers prepared materials with high specific surface areas and well-defined pores to improve the capacitance. Others synthesized the core-shell nanostructured materials with high stability and high rate capability. In general, the core materials are the main active component with specific functions, while the shell materials serve as a protective layer to enhance the core materials performance or to produce new properties. The unique structure could not only protect the active materials from aggregation, but also be regarded as an effective strategy to simultaneously obtain high utilization and high mass-loading of the electrode materials for supercapacitors. Besides the spherical shape, the core-shell nanostructures materials have a variety of other shapes, such as prism, octahedron, wire, rod, cube, tube, *etc.* [55] These core-shell nanomaterials of different shapes can provide short diffusion path and high active surface area to ions and electrons and may produce a synergistic effect of each component, resulting in high capacitance, low internal resistance, remarkable rate capability, and excellent stability. [56] However, the ideal core-shell structured nanomaterials in supercapacitors have many requirements for shell materials: 1) maintain structural integrity and limit volume expansion; 2) prevent outside environmental from polluting the active core; 3) strengthen or produce new chemical or physical properties; 4) protect the core from aggregation; 5) permit rapid transport for electrons and ions, and *etc.*

2.1.1. Core-shell structured nanomaterials for double layer capacitors

Many researchers are dedicated to the exploration of core-shell structured nanomaterials for EDLCs. Liu et al. [52] synthesized core-shell structures carbon nanospheres, and used them as the electrode of the supercapacitor. The results showed that the core-shell structures carbon nanospheres had high specific capacitance, high current density, and excellent long-term cycle stability. Meanwhile, there is a synergistic effect when porous carbon materials and other carbon materials are combined together. Based on the theory of electrochemical double layer, the capacitive performance could be improved when porous carbon materials were combined with nanocarbons, such as CNTs [57,58], graphene [59], and carbon nanofibers (CNFs) [60]. Using a simple sol-gel method, Qian et al. [61] synthesized multiwall CNT@MC (MWNT@mesoC) composite, which exhibited excellent electrochemical performance with greatly improved specific capacitance from 6.8 to 60.2 F g^{-1} in 6.0 M KOH. Good rate performance and high cyclic stability (94% after 1000 cycles) were also obtained (Fig. 2).

Recently, graphene has attracted tremendous attention due to its high theoretical surface area (*ca.* 2600 m^2 g^{-1}), which is substantially higher than that of single-walled CNTs, most carbon blacks and AC [62]. However, graphene sheets may easily re-accumulate and generate irreversible agglomerates, damaging its energy storage performance. Therefore, graphene is often combined with other carbon materials, such as carbon nanofibers (CNFs), CNTs and hierarchically porous carbon. Lin et al. [63] synthesized novel heterostructure of CNTs@graphene oxide nanoribbons utilizing graphene oxide nanoribbons as the shell and the MWNT as the core. The specific capacitance (252.4 F g^{-1}) of this supercapacitor electrode was greatly improved and superior for the supercapacitor electrodes compared with commercial GNP (19.8 F g^{-1}) and MWN/CNT (39.7 F g^{-1}) because the surface area of the contact to the electrolyte ions and the pore-size distribution can greatly influence the capacitance. For instance, core-shell porous carbon@CNT ternary carbon material showed superior capacitive performance because the developed porous structure could provide more diffusion paths, which would significantly promote the ability of ion transport/charge storage [64]. The electrode materials of EDLCs can be used in some mobile and stationary systems that require high power pulses. Therefore, There is a need to continuously improve the surface area or select more appropriate porous structures to enhance the specific capacitance of carbon-based core-shell structured materials [65–75]. Another method of enhancing the capacitance is to combine the carbon materials with metal oxides/conducting polymers, as described in the following section. They can quickly store energy in virtue of their low time constant. Unfortunately, a high internal series resistance among carbon materials is produced which makes them suffer from high resistivity and low energy density [76]. The surface area inaccessible to electrolyte ions will also impede the energy storage performance of core-shell structured nanomaterials [77]. Therefore, future researches need to focus on rational pore distribution and higher specific surface area to improve overall conductivity and capacitance without compromising stability.

2.1.2. Core-shell structured nanomaterials for pseudocapacitors

Pseudocapacitors that store charges through a Faradaic process have attracted much attention due to their higher energy density compared to EDLCs [78–80]. The component and the structure of the electrode materials play important roles in the charge-discharge process between the electrolyte ions and active materials. Among all multicomponent nanomaterials, core-shell structured nanomaterials are one of the most promising high-quality materials due to the full contact, massive active sites, fast ion diffusion and porous structures. Among all

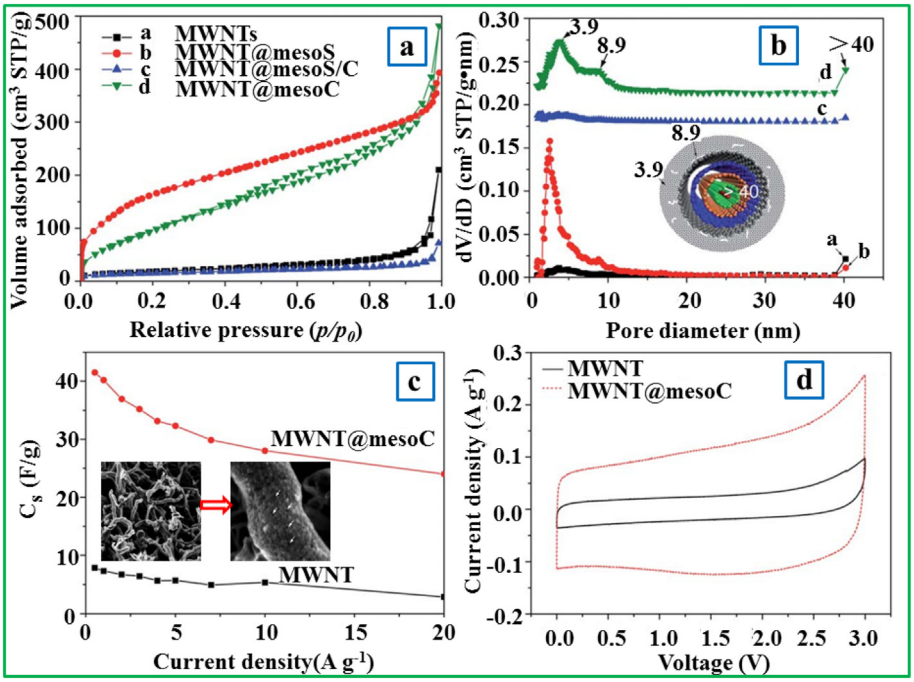

Fig. 2. (a) Nitrogen sorption isotherms, (b) pore size distribution curves, (c) the specific capacitance as a function of current density of the pristine MWNTs@mesoC and MWNTs electrode materials in 1.0 M $(C_2H_5)_4NBF_4$/PC electrolyte, (d) cyclic voltammograms at a rate of 5 mV s^{-1}. Adapted from ref. [61]. Copyright (2011) The Royal Society of Chemistry.

core-shell structured nanomaterials, conducting polymers (CPs) (*e.g.,* polythiophene [PTh], polypyrrole [PPy], polyaniline [PANI], and their derivatives) are suitable materials for pseudocapacitors because of their unique properties (*e.g.,* low cost and small dimensions, high storage ability/porosity and high voltage window, and controllable redox activity) [21,81–85]. Jabeen et al. [86] synthesized unique $NiCo_2O_4$@PANI core-shell nanorod arrays (NRAs), which were used as the electrode material for pseudocapacitors and attained a satisfactorily good rate capability, high capacitance and cycling stability. In addition, note that the work environment of CPs is harsh and needs a tough potential window, namely, "limited scope". Beyond the "limited scope", the polymer can be degraded in most positive potentials, and the polymer can be turned into an insulating state when the potential is too negative. Hence, it is vital to select a suitable potential range for pseudocapacitors. Ma et al. [87] used the layer-by-layer process to prepare a novel material containing PPy, ZnO and MnO_2. The charge transfer impedance of the composite was decreased, and the electrochemical property was improved (~1281 F g^{-1}/2.5 A g^{-1}). Generally, poly(3,4-thylene-dioxythiophene) is used as an alternate material for pseudocapacitors because of its high stability [88,89]. Many researchers find it perplexing that the shrinking and swelling of CPs in the deintercalation/intercalation process result in weakening of mechanical strength of electrode and the decline of capacitance during cycling. To solve these shortcomings, some effective strategies have been investigated, including improving the morphologies and structures of CP materials, hybridizing pseudocapacitors, and fabricating composite electrode materials. For instance, Hu et al. [90] synthesized hierarchical manganese dioxide/poly (3,4-thylene-dioxythiophene) (PEDOT) core-shell nanoflakes on CNF derived from ramie (RCFs) (Fig. 3a-d). The hybrid electrode material achieved a high specific capacitance with 922 F g^{-1} (1 A g^{-1}) and a remarkable rate capability retention of 345 F g^{-1} (40 A g^{-1}). They also found that the specific capacitance of the CP device after 10,000 cycles at a charge-discharge density of 8 A g^{-1} only slightly decreased, retaining approximately 83% of the initial capacitance. The performance of CPs can be significantly improved because of the unique merits of core-shell structure electrode material.

Generally, metal oxides have better electrochemical stability than CPs and higher energy density than traditional carbon materials for pseudocapacitors. They can be used as a substitute for carbon materials as new material for energy storage, and they can also produce faradaic reactions between ions and electrode materials within a suitable potential window [93]. For metal oxides in pseudocapacitors applications, the general requirements are (i) good conductivity, (ii) existence in two or more oxidation states, and (iii) the protons can be out of the lattice on oxidation (freely insert the oxide lattice on reduction), permitting facile conversion of $O^{2-} \leftrightarrow OH^-$. Until now, those materials with core-shell structure, including nickel oxides, manganese oxides and other metal oxides, have been widely used in pseudocapacitors applications. Since an early study by Goodenough and Lee in 1999 [94], MnO_x has been concerning. It was regarded as a promising alternative materials for pseudocapacitors applications because of low toxicity, environmental safety, and low cost as well as good specific capacitance [87,95–97]. Both chemical factors and physical properties, such as the crystallinity, crystal structure, specific surface area and pore structure, can affect the electrochemical performance of Mn oxides. For example, the stability of Mn oxides is primarily decided by their microstructure [98]. Liu et al. [99] used nano-networks of a MnO_2/Ni core-shell composite as a pseudocapacitor electrode material, and it exhibited excellent electrochemical performance and demonstrated a capacitance of 214 F g^{-1}, according to galvanostatic testing in a stable current density of 20 A g^{-1}. Many researchers have also emphasized the hierarchical core-shell structure to maximize the specific surface area of metal oxides [11,95,100]. The construction of peculiar hierarchical core-shell nanostructures plays a significant role in the effective enhancement of the stability and the rate capacity. The cycling stability achieved 98.1% after 10,000 discharge-charge cycles, higher than those reported in the literature [101–103].

Generally, NiO and $Ni(OH)_2$ composites are considered to be promising materials in pseudocapacitors applications because of the wide potential window, high specific capacitance, inexpensive raw materials and easy control of the binary oxides composition [104]. The synthesized nano-NiO composites involve nanoflakes, nanosheets, nanocolumns, nanoring, and hierarchical nanoflowers as well as hollow nanospheres [105–109]. However, it is challenging to use NiO-based electrode materials for the pseudocapacitors because of its poor cycle performance and high resistivity. Therefore, the hierarchical porous

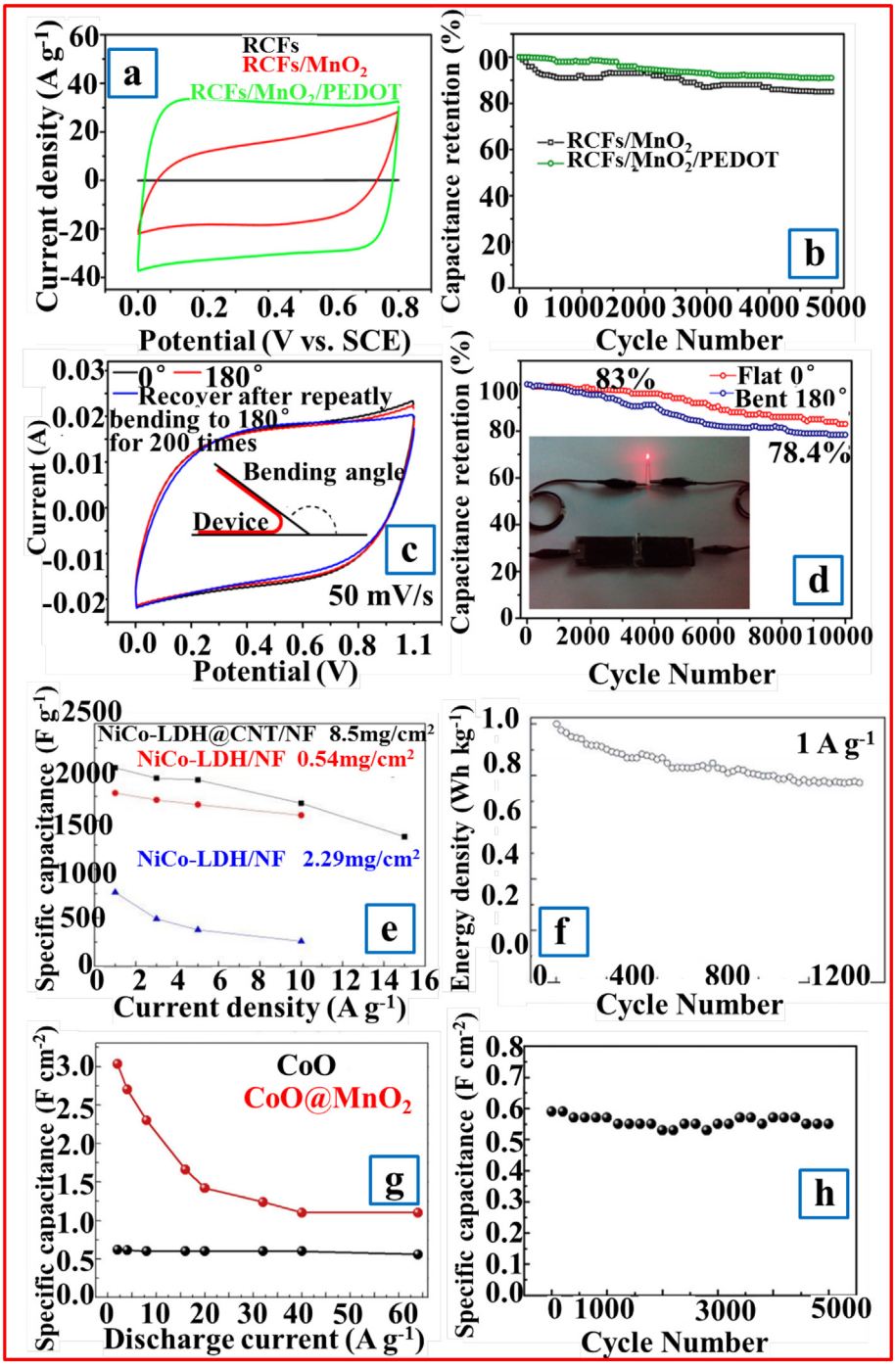

Fig. 3. The electrochemical performance of RCFs/MnO_2/PEDOT: (a) CV curves under 50 mV s^{-1}, (b) the plot of capacitance retention vs cycle number at a current density of 10 A g^{-1}; The electrochemical performance of the RCFs/MnO_2/PEDOT electrode (c) CV curves at 50 mV s^{-1} for the device under different bending states, (d) the plot of capacitance retention vs cycle number at a current density of 8 A g^{-1}. Adapted with permission from ref. [90]. Copyright (2016) American Chemical Society. The electrochemical performance of NiCo-LDH@CNT/NF and NiCo-LDH/NF electrodes: (e) specific capacitance comparison of two electrodes at different mass loadings, and (f) cycling stability of the ASC device at 1 A g^{-1}; The electrochemical performance of CoO and CoO@MnO_2: (g) specific capacitances s of CoO and CoO@MnO_2 at different current densities, (h) cycle stability tested by galvanostatic charge/discharge in 16 mA cm^{-2}, Adapted from ref. [91, 92]. Copyright (2015) The Royal Society of Chemistry; Copyright (2016) Elsevier Ltd., respectively.

core-shell structured nanomaterials of nickel oxides have been highly developed [110]. As a result, the capacitance retention ratio of nickel oxide greatly improved because the hierarchical porous core-shell structure could admit ions to easily pass through the electrode/electrolyte interface. Recent studies have found that the specific capacitances of $Ni(OH)_2$ composite are significantly higher than NiO [111]. Jiang et al. [97] synthesized $Ni(OH)_2$@MnO_2 nanowires, which were used as the electrode material for pseudocapacitors. This electrode material could be used in both neutral electrolytes and alkaline electrolytes and showed good cycling stability because of the synergistic effect between the shell and core. Yin et al. [112] found that NiCo-O/$Ni(OH)_2$ core/shell electrodes had great practical values in the fields of pseudocapacitors. Beyond that, other transition metal-based core-shell materials also have desirable properties, such as Co_3O_4/$Co(OH)_2$, Fe_3O_4, ZnO, MoO_3, and CuO, *etc.* [113–115]. For example, prepared 3D Co@Co_3O_4 nanonetwork exhibited high capacitance (1049 F g^{-1}) [80]. Aiming to further improve the performance of transition metal-based core-shell materials, some optimizations have been performed by doping with other

metal elements. For instance, Hong et al. [45] synthesized Co_3O_4@Co-Ni-sulfides nanowire arrays as the electrode material for pseudocapacitors. This electrode material obtained a higher specific capacitance of 1844 F g^{-1} at 5 mA cm^{-2}. Fe_3O_4@SnO_2 core-shell nanorod film was prepared and exhibited good cycling stability [116]. Generally, compared to Co_3O_4-based materials, $Co(OH)_2$-based materials can provide much higher specific capacitances. Recently, other metal oxides have also been studied extensively. Fe_3O_4@SnO_2 core-shell nanorod film was prepared by Li et al. [116] and used as a pseudocapacitor electrode, which exhibited good cycling stability. The noble metals of Au and Ag have attracted considerable attention recently due to their high electrochemical stability [117]. In particular, Yuksel et al. [118] prepared a novel hybrid composite consisting of silver nanowire core with MoO_2 shell as pseudocapacitors electrodes. The electrode material improved the specific capacitance and exhibited excellent ability retention after 5000 cycles. Many other metal oxide materials, such as ZnO, MoO_2, and CuO, have also been studied as electrode materials for pseudocapacitors [113–115]. Basically, the redox activity and surface area are improved by regulating the materials morphology or combining them with other materials. Pseudocapacitors materials, particularly CPs, are still subject to some problems, such as significant volume changing in the process of charging and discharging and poor cyclic stability.

2.1.3. Core-shell structured nanomaterials for asymmetric supercapacitors

The design of novel advanced supercapacitors should possess higher energy and operating voltage in the future [119]. Recently, asymmetric supercapacitors have attracted much attention due to their high cell voltage, consisting of a capacitor-type electrode as power source and a battery-type Faradic electrode as an energy source because it can significantly enhance energy density and improve specific capacitance by exploiting the two electrodes, with different potential windows, to enhance the operation voltage [120,121]. Various asymmetric supercapacitors have been widely studied, such as AC//$LiMn_2O_4$ [122], AC//MnO_2 [123], AC//graphite [124], CNT//TiO_2 [125], *etc.* The performance of asymmetric supercapacitors directly depends upon the properties and structure of the super-capacitive electrode materials [126]. Therefore, the construction of core-shell structured nanomaterials with the transition metal oxides has attracted the concern of the researchers due to their superior achievable oxidation states, electrical conductivity, and high electrocatalytic activity.

As for the cathode material of asymmetric supercapacitors, carbon materials are a widely utilized cathode material, due to their relatively good electrical conductivity and high surface area [127]. To satisfy the demand of high current density in a large charge/discharge process, carbon materials should have a high surface area and short pore length, as well as narrow pore size distribution with interconnected pore structure, because it can provide not only a good rate capability but also an enhanced energy, thereby producing an enormous amount of double layers to expedite the transmission of electrolyte ions [128]. For the positive electrode material, the core-shell structure pseudo-capacitive material with high electrical conductivity and smaller nanometer-sized particles, such as MnO_x, CoO_x, FeO_x and NiO_x, are particularly attractive because of their easy fabrication, tunable surface, desirable pseudocapacitive and structural properties, abundant nature, and high theoretical capacitance [129,130]. For example, the 3D core-shell structured NiCo-LDH@CNT (LDH- layered double hydroxide) and APDC (activated polyaniline-derived carbon) were used as positive electrode and negative electrode, respectively [91]. The positive material exhibited high capacitance of 2046 F g^{-1} at 1 A g^{-1} and 1335 F g^{-1} at 15 A g^{-1}, with a mass loading of 8.5 mg/cm^{-2}, respectively (Fig. 3e). It also exhibited excellent cycle stability (Fig. 3f). It is remarkable that the NiCo-LDH@CNT/NF//APDC/NF supercapacitor device showed a maximum power density of 8.7 kW kg^{-1} with an energy density of 41.7 Wh kg^{-1} and a maximum energy density of 89.7 Wh kg^{-1} at a working voltage of 1.75 V when combined with APDC-based negative electrode. CoO@MnO_2 nanowire@nanosheetarrays (NNSs) were tested in asymmetric hybrid cell configurations, in which the CoO@MnO_2 NNSs exhibited a significantly improved specific capacitance of 3.03 F cm^{-2} (~1515 F g^{-1}) with a broad potential window of 0.8 V at 2.0 mA cm^{-2}, which was much better than the most reported Co_3O_4-based core-shell structure NNAs electrodes (Fig. 3g) [92]. Meanwhile, the energy density of asymmetric supercapacitor devices with long-term cycling capacity can retain 96.5% of the initial capacitance after 5000 cycles (Fig. 3h). We can also see the electrochemical performance of asymmetric supercapacitors compared to EDLCs and pseudocapacitors with different core-shell structured nanomaterials in Table 1. The electrochemical performance of pseudo-capacitive materials with CPs and transition metal oxides can be enhanced through combination with carbon materials. The asymmetrical supercapacitors have been profoundly studied to enhance the overall cell voltage, power densities and energy of electrode materials. However, the coordinating optimum charge-discharge rates between pseudo-capacitive materials and carbon material must be considered fully in the practical application of asymmetric supercapacitors.

2.2. Core-shell structured nanomaterials for lithium battery

The development of rechargeable lithium-ion batteries (LIBs) with high energy densities has received considerable attention. However, the electrode materials of LIBs are still suffering from many obstacles, such as the slow Li^+ diffusion and high resistance at the electrolyte/electrode interface. To solve these difficult problems, great efforts have been devoted to the development of advanced active electrode materials with good thermal/mechanical stability, high power/energy density, low cost and environmental friendliness for practical applications. Among all the research, various core-shell structured nanomaterials have aroused great attention because they can improve the reactivity and conductivity of Li^+ ion/electron, accelerate charge across the electrolyte/electrode interface and shorten the Li^+ extraction/insertion pathway. In this system, the shell also plays a vital role in enhancing the performance of active core materials. To enhance the electronic conductivity, besides traditional carbon materials like graphite, metal/metal oxides and electrically conductive polymers are also suitable candidates for shell materials. To solve the problem of volume change, polymers, amorphous carbon, and other flexible materials can be selected due to their abundant pore structure. Thus, the selection of shell materials should meet the following requirements: 1) it can improve the electronic conductivity of active cores; 2) it should provide a buffering space for the enormous contraction/expansion; 3) it can protect the active core materials from directly contacting the electrolytes or air and avoid the loss of active ingredients; 4) it can react with HF produced from electrolytes to maintain a stable and high performance of active cores (the shell always acts as a HF scavenger). Since related content as introduced in a 2011 review [148], here we mainly review studies from 2011 to the present and summarize the electrochemical performances of core-shell structured nanomaterials for LIBs.

2.2.1. Lithium transition metal oxides

Lithium transition metal oxides (LTMO), such as layered $LiCoO_2$, $Li_4Ti_5O_{12}$ and spinel-type $LiMn_2O_4$, are the typical and most promising materials. The strong M-O bonds (where M = Co, Fe, Ni, Sn, Cu, *etc.*) can provide favorable Li^+ transport paths and electrons, and insure the stability of the structure in the process of lithiation/delithiation. In particular, the LTMO with core-shell structure is a promising material to increase the yield of Li^+ and facilitate the electronic transport, restrict or accommodate the volume change. Carbon coating is considered to be a feasible method because of its low cost, easy preparation, low resistance and environmental friendliness. For instance, Zhong et al. [149] synthesized a $LiFe_{0.5}Mn_{0.3}Co_{0.2}PO_4$@C composite through a simple rheological phase reaction, in which the carbon source was stearic acid. This symmetrical carbon layer achieved a high discharge capacity

Table 1
Summary of the performances of core-shell structured nanocomposites anodes for supercapacitors (reported in the literature since 2011).

Type	Active material	Synthesis method	Eenrgy density	Capacitance[1]	Capacitance[2]	Cycle	Ref
Double layer capacitors	N-doped active carbon fiber@graphene	Dipcoating	50.0 W kg^{-1} (17.1 W h kg^{-1})	552.8 F g^{-1} (0.1 A g^{-1})	373.2 F g^{-1} (20 A g^{-1})	2000 (90%)	[131]
	Sea urchin-like core-shell hierarchical porous carbon	One-pot cooperative assembly	–	230 F g^{-1} (0.5 A g^{-1})	103 F g^{-1} (10 A g^{-1})	10,000 (95.02%)	[132]
	Graphene and core-shell activated carbon coated carbon nanotube	Hydrothermal	–	193 F g^{-1} (10 mV s^{-1})	138 F g^{-1} (5000 mV s^{-1})	6000 (100%)	[64]
	Multiwall CNT@ mesoporous carbon	Sol–gel methods	–	60.2 F g^{-1} (1 A g^{-1})	36 F g^{-1} (20 A g^{-1})	94% (1000)	[61]
Pseudocapacitors	Multi-walled CNT@ graphene oxide nanoribbons	Layer-by-layer hydrothermal	–	311.9 F g^{-1} (5 mV s^{-1})	80.7 F g^{-1} (1000 mV s^{-1})	95% (1000)	[133]
	Co_3O_4@$CoMoO_4$ nano-pine forest arrays		400 W kg^{-1} (45.2 W h kg^{-1})	1902 F g^{-1} (1 A g^{-1})	1200 F g^{-1} (10 A g^{-1})	5000 (99%)	[134]
	Ag nanowire@$Ni(OH)_2$	Electrodeposition	–	1165.2 F g^{-1} (3 A g^{-1})	863.0 F g^{-1} (50.0 A g^{-1})	3000 (93%)	[135]
	Highly porous honeycomb manganese oxide@carbon fibers	Hydrothermal+ in situ redox replacement reaction	12,000 W kg^{-1} (10.0 W h kg^{-1})	295.24 F g^{-1} (100 mA g^{-1})	58.28 F g^{-1} (500 mA g^{-1})	3000 (96.4%)	[136]
	Hollow SnO_2@Co_3O_4@ graphene foam	Deposition+ hydrothermal	–	530 F g^{-1} (0.5 A g^{-1})	350 F g^{-1} (10 A g^{-1})	–	[137]
	$NiCo_2O_4$@$MnMoO_4$ core-shell flowers	Hydrothermal	7000 W kg^{-1} (126.4 W h kg^{-1})	1118 F g^{-1} (1 A g^{-1})	746 F g^{-1} (10 A g^{-1})	5000 (92.3%)	[138]
	3D NiO@MnOOH	Electrodeposition+chemical bath deposition	17.1 W kg^{-1} (80 W h kg^{-1})	1890.5 F g^{-1} (1.7 A g^{-1})	1223.3 F g^{-1} (20 A g^{-1})	5000 (105.7%)	[139]
Asymmetric supercapacitors*	3D ordered core-shell macroporous Mn/Mn oxide	Electrodeposition hydrothermal	47.3 W kg^{-1} (79 W h kg^{-1})	1200 F g^{-1} (10 mV s^{-1})	370 F g^{-1} (500 mV s^{-1})	2000 (96%)	[140]
	Co_3O_4@$CoMoO_4$//CNTs		6400 W kg^{-1} (37.0 W h kg^{-1})	128 F g^{-1} (3 A g^{-1})	68 F g^{-1} (8 A g^{-1})	3000 (98.5%)	[134]
	$NiCo_2S_4$@$Co(OH)_2$//AC	Hydrothermal+ electrodeposition	400 W kg^{-1} (35.89 W h kg^{-1})	9.6 F cm^{-2} (2 mA cm^{-2})	6.4 F cm^{-2} (32 mA cm^{-2})	5000 (70.0%)	[141]
	Hirearchically porous MnO_2 nanflakes@PPy nanowires//AC	Sol-gel	9000 W kg^{-1} (17.1 W h kg^{-1})	276 F g^{-1} (2 A g^{-1})	200 F g^{-1} (20 A g^{-1})	6000 (90.3%)	[142]
	ZnO@MnO_2 nanofiber//AC	Electrodeposition	650 W kg^{-1} (17.0 W h kg^{-1})	907 F g^{-1} (0.6 A g^{-1})	210 F g^{-1} (35 A g^{-1})	2500 (97%)	[143]
	A-Fe_2O_3@PANI//	Electrodeposition	120.51 mW cm^{-3} (0.35mWh cm^{-3})	2.02 mF cm^{-3} (5 mV s^{-1})	0.78 mF cm^{-3} (100 mV s^{-1})	10,000 (95.7%)	[144]
	Hierarcal Fe_3O_4@Fe_2O_3 nanorod arrays//Fe_3O_4@MnO_2	Hydrothermal+ electrodeposition	15.6 mW cm^{-3} (0.83mWh cm^{-3})	1.206 mF cm^{-3} (5 mV s^{-1})	0.55 mF cm^{-3} (200 mV s^{-1})	5000 (92%)	[145]
	MnO_2@$NiMoO_4$//Porous carbon	Hydrothermal	450 W kg^{-1} (12.5 W h kg^{-1})	186.9 F g^{-1} (10 mV s^{-1})	46.5 F g^{-1} (100 mV s^{-1})	20,000 (132.7%)	[146]
	Homogeneous core-shell $NiCo_2S_4$//	Hydrothermal	2.47 W kg^{-1} (10.6 W h kg^{-1})	1948 mF cm^{-2} (5 mA cm^{-2})	1546 mF cm^{-2} (20 mA cm^{-2})	5000 (94%)	[147]

Capacitance[1]: Capacitance at low current density.
Capacitance[2]: Capacitance at high current density.
* a//b a-positive electrode, b-negative electrode.

(146.7 mAh g^{-1} at 0.1C) and maintained 90.6% after 100 cycles with ability retention because the existence of carbon shell avoided the active component from corroded by electrolyte. Meanwhile, carbon-coated $LiFePO_4$ was synthesized by Wang and coworkers using a solid-liquid reaction milling method [150] and exhibited good electrochemical performance (131.3 and 163.6 mAh g^{-1} under different temperature). However, carbon-coated lithium transition metal oxides electrode materials have been rarely reported because the active metals, particularly high-valence metal, might be reduced by the CO or H_2 in the carbonization process of hydrocarbons [151]. Accordingly, researchers have been working on developing carbon-coated layer substitutes, which would greatly improve the electrochemical behaviors.

$LiFePO_4$ and vanadium-based phosphate ($LiVOPO_4$, $Li_3V_2(PO_4)_3$ and $LiVPO_4$) are one of the most promising materials due to their abundant raw materials, good thermal stability and good electrochemical performance. However, poor ionic and electronic conductivity limit their wide application. To enhance the electronic conductivity of Li^+ inherently, an effective method is to cover a layer of carbon shell on the surface. For example, preparation of $LiFePO_4$ powder with a high conductivity carbon shell through mechanical mixing, such as acetylene black, graphite, mesocarbon microbead (MCMB), can produce a rough core-shell structure. However, the active sites are not completely encapsulated by the carbon shell, and many naked areas are directly exposed to electrolytes or air [150]. The strategy can avoid these results by using organic matter as carbon source. Liu et al. [152] fabricated $LiFePO_4$@C composite by using organic matter as a carbon source, showing prominent initial capacity (161 mAh g^{-1}/0.1 C), excellent rate discharge ability (135 mAh g^{-1}/5C) and high cycling retention (99.6% after 100 cycles). Despite the fact that the low conductivity can be enhanced by being fully covered with carbon materials as mentioned above, the low tap density and high cost of nanomaterials still limit their large-scale practical application. Xu et al. [153] synthesized $LiFePO_4$@C using ascorbic acid as carbon source which exhibited excellent electrochemical performance. This composite produced inter-connective pores that benefited electrolyte adsorption and dramatically decreased the diffusion pathway of Li^+. The $LiFePO_4$@C composites showed excellent electrochemical performance. However, both $LiCoPO_4$@C and $LiMnPO_4$@C possessed higher potential (4.1 V and 4.8 V *vs.* Li^+/Li) than $LiFePO_4$ (3.4 V *vs.* Li^+/Li) [154–156]. Cheng et al. [157] synthesized $LiMnPO_4$@C nanocomposites which produced a high capacity of 156 mAh g^{-1} and superior stability because the uniformly covered carbon layer could prevent $LiMnPO_4$ from an HF attack and even lead to lesser manganese dissolution, lower resistance and optimal conductivity. Meanwhile, $Li_3V_2(PO_4)_3$ has the same low conductivity as $LiFePO_4$. The issue can also be resolved by doping or covering the conductive materials. Duan [158] synthesized $Li_3V_2(PO_4)_3$@C nanocomposites by using ascorbic acid and PEG-400 as a carbon source, using a hydrothermal-assisted sol-gel method. It exhibited a prominently long cyclic stability and high rate capability. Fig. 4a

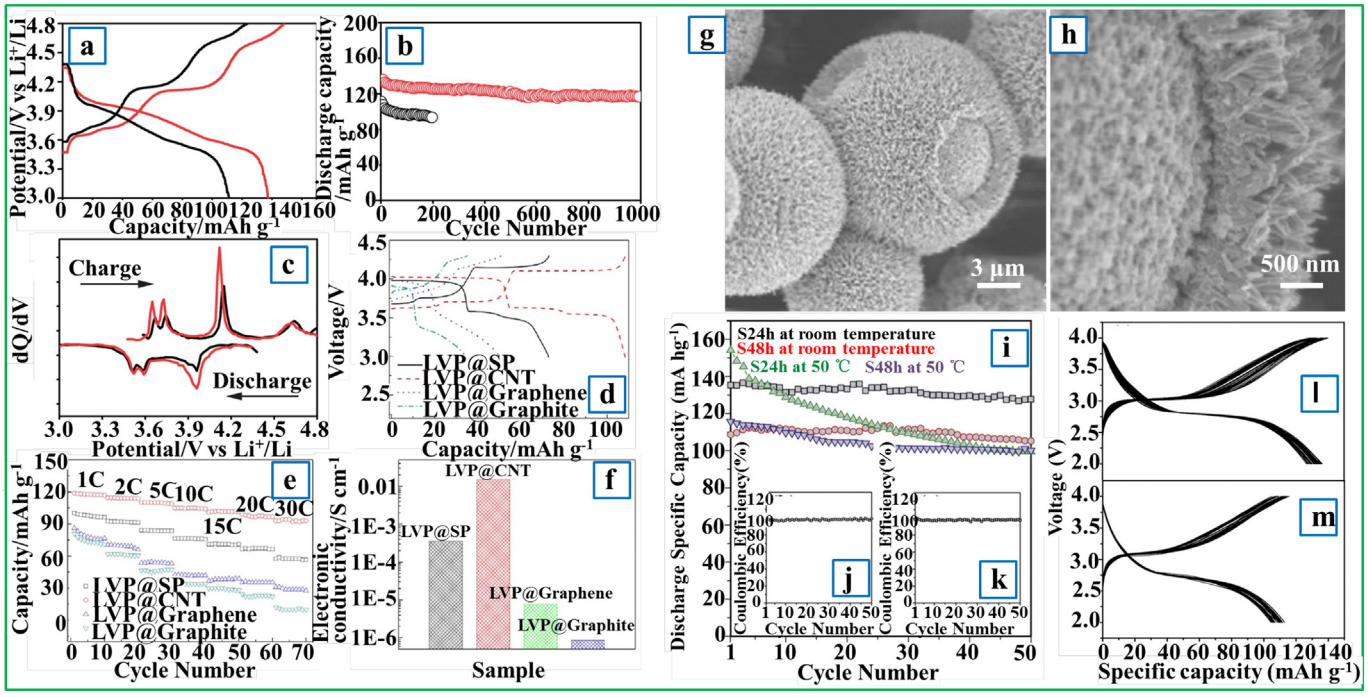

Fig. 4. The electrochemical performance of M-LVP and N-LVP: the initial charge/discharge profiles (a), the cycling performance (b), the corresponding differential capacity plots (c) at 5 C; The electrochemical performance of LVP@CNT: cycling performance at 5 C charge and 100 C discharge rates (d), corresponding cycling performances of LVP@Graphite, LVP@Graphene, LVP@CNT, and LVP@SP at 5 C rate (e), and electronic conductivities (f); Adapted from ref. [158, 160]. Copyright (2013) The Royal Society of Chemistry; Copyright (2015) American Chemical Society, respectively. (g) SEM images of S24 h (react time) and (h) cross-sectional TEM images, (i) variation of discharge capacities versus cycle number for S24 h and S48 h at room temperature and 50 °C, and their coulombic efficiency at room temperature (j and k), (l) charge/discharge curves of S24 h and (m) S48 h between 2.0 and 4.0 V at 10 mA g^{-1} under room temperature. Adapted from ref. [161]. Copyright (2011) Elsevier B.V.

shows that the nanocomposites with different crystalline phase have a similar charge-discharge profile shape. In particular, N-LVP (the red line) exhibited a discharge capacity of 138 mAh g^{-1} at 5 C within a voltage range of 3–4.8 V, and the capacity retention was 86.0% after 1000 cycles. However, the capacity of M-LVP (the black line) had faded to 84.0% after 200 cycles, with an initial discharge capacity of 111.0 mAh g^{-1} (Fig. 4b). The corresponding d*Q*/d*V* plots suggested that all three Li ions are mobile during discharge-charge process. The peaks of N-LVP (the red line) are sharper and have a higher intensity, suggesting easier insertion/extraction of Li^+ (Fig. 4c). Zhang et al. [159] anchored the monoclinic $Li_3V_2(PO_4)_3$@C particles to graphene sheets using the *Pechini* method, in which the graphene was first suggested to use as a chelating agent. The composite showed excellent electrochemical performance and provided high capacities (104, 91 mAh g^{-1}/5 C and 85 mAh g^{-1}/30 C, respectively). Moreover, the cycling stability was also enhanced in voltage window of 3.0–4.8 V, and the initial capacity remained 83% after 100 cycles. Mao et al. [160] synthesized the $Li_3V_2(PO_4)_3$@CNT nanocomposites through an in situ synthesis strategy (LVP@CNT). It exhibited a high rate ability and long cyclic stability and provided a remarkably reversible capacity (91.94 mAh g^{-1}/100 C) (Fig. 4d). Even after 200 cycles, the capacity retention could retain 91.28% at a 5C rate compared to different carbon materials. The initial reversible capacity could even remain 80.0% after 382 cycles, and the Coulombic efficiency was hardly reduced (Fig. 4e). Meanwhile, LVP@CNT had the highest electronic conductivity (~10^{-2} S cm^{-1}) compared to that of its counterparts; this outcome was highly related to its intrinsic properties (Fig. 4f).

The electrolytes have an important influence on the performance of coating materials. The traditional electrolytes primarily include carbonic esters and lithium salt ($LiPF_6$), which are easily affected by damp air. In truth, $LiPF_6$-based electrolytes with a little water will greatly accelerate the decomposition of $LiPF_6$ salt along with HF generation [162]. The active component will be corroded by HF; meanwhile, the solvent will be oxidized to produce a stable solid electrolyte interface sheeting by the high valence metals. To inhibit the corrosion of active component, electrolyte additive are widely studied, which can generate effective solid electrolyte interface sheeting. Simultaneously, modifying the surface to form a "shell" is also a feasible strategy because it can guarantee the direct contact between an active component and electrolyte and prevent co-intercalation and corrosion by producing a protective layer. Furthermore, the dense passivation layer could also enhance the cyclic stability and stabilize the crystalline lattice. Cho et al. [163,164] earlier adopted a strategy to modify the surface by covering inactive metal oxides on $LiCoO_2$ particles. They found that the dense inactive metal layer could significantly impede the change of lattice constant and inhibit the unwanted phase transition during electrochemical cycling. Li et al. [161] synthesized the core-shell structure $Li_4Mn_5O_{12}$@Li_2MnO_3 using a facile $LiNO_3$ flux method. The TEM image of the nanocomposite revealed that microspheres were a kind of core-shell structure (Fig. 4g). A layer nanorod with lengths of 200–300 nm, and diameters of 20–30 nm grew on the surface of the microsphere, which constituted the shell of the microsphere (Fig. 4h). In addition, as shown in Fig. 4i, S24 (prepared for 24 h) exhibited good cycle stability with initial capacity of 136.0 mAh g^{-1}, which remained 94.2% after 50 cycles. The two constructed devices showed excellent coulombic efficiencies and demonstrated highly reversible insertion/extraction of Li^+ during discharge and charge process (Fig. 4j and k). Meanwhile, the discharging and charging behaviors of the nanocomposites S24 h and S48 h (prepared for 24 h and 48 h) exhibited the typical characteristics of a $Li_4Mn_5O_{12}$ electrode at the current density of 10 mA g^{-1} (Fig. 4l and m). These results indicated that the Li_2MnO_3 shell could enhance the cycling stability of electrode materials.

2.2.2. Si, Sn and alloys with carbon shells

Silicon-based materials have obtained tremendous attention due to their high theoretical capacity of nearly 4200 mAh g^{-1}. It is approximately 11 times as much capacity as traditional graphite (372 mAh g^{-1} for LiC_6). However, the large volume expansion/contraction of electrode

materials seriously limits the practical application, resulting in the breakdown of the electrically conductive network and pulverization of the electrode [165]. To solve these issues, researchers emphasized the following three strategies: usage of effective binders, and preparation of nanoscale materials and construction of core-shell structures. For instance, roughly carbon-coated Si-based materials were prepared through various strategies and exhibited excellent capability (500–900 mAh g^{-1}) [166–168]. Ascribing to the large surface stress, nanoscale Si-based materials were hard to wrap into carbon particles without pretreatment, therefore, micron-sized Si-based materials were often used to prepare core-shell structured nanomaterials with carbon shell. On the other hand, since the nanoscale Si-based powder possesses higher irreversible capacity and more side reactions, they can shorten the path lengths of Li-+ transport, increase interfacial areas, and improve accommodation of the volume change. Hence, it is meaningful to develop a simple and low-cost synthesis method of nanoscale Si-based powder with carbon shell. Kim et al. [169] synthesized carbon-coated Si nanocomposites through thermal decomposition. The Si-based anode materials exhibited excellent rate capability (1700 mAh g^{-1}), stable cycle performance (remain 1200 mAh g^{-1} after 300 cycles) due to the existence of carbon shell. Similarly, Zhou et al. [170] synthesized Si@C core-shell composites through a flexible and tunable route, which showed large volume variations and poor cycle stability. The combination of carbon and silicon is essential to improve the performance of the Si-based electrode materials. In addition, Si@C nanocomposites can also be synthesized through scattering silicon nanoparticles in carbon composites with immediate carbonization. These composites showed high reversible capacities (1000 mAh g^{-1}) [171]. Si@C nanotubes and nanowires exhibited better high-rate performances and higher reversible capacities than pure Si@C nanoparticles. Carbon-coated 1 D materials, particularly when nanowires/nanotubes are regularly coated the collector, can provide good accommodation and improve electronic transport capacity [172]. It is also easy to coat Sn and Sb-based composite with a carbon shell. This composite can provide a larger expansion space and high electronic transfer rate, leading to high cycling stability and energy density. Li et al. [173] synthesized yolk-shell Sn@C composite (SCE) using a facile method. The synthetic procedure of the composite is shown in Fig. 5a. The hollow SnO_2@C was first fabricated as precursors through a simple

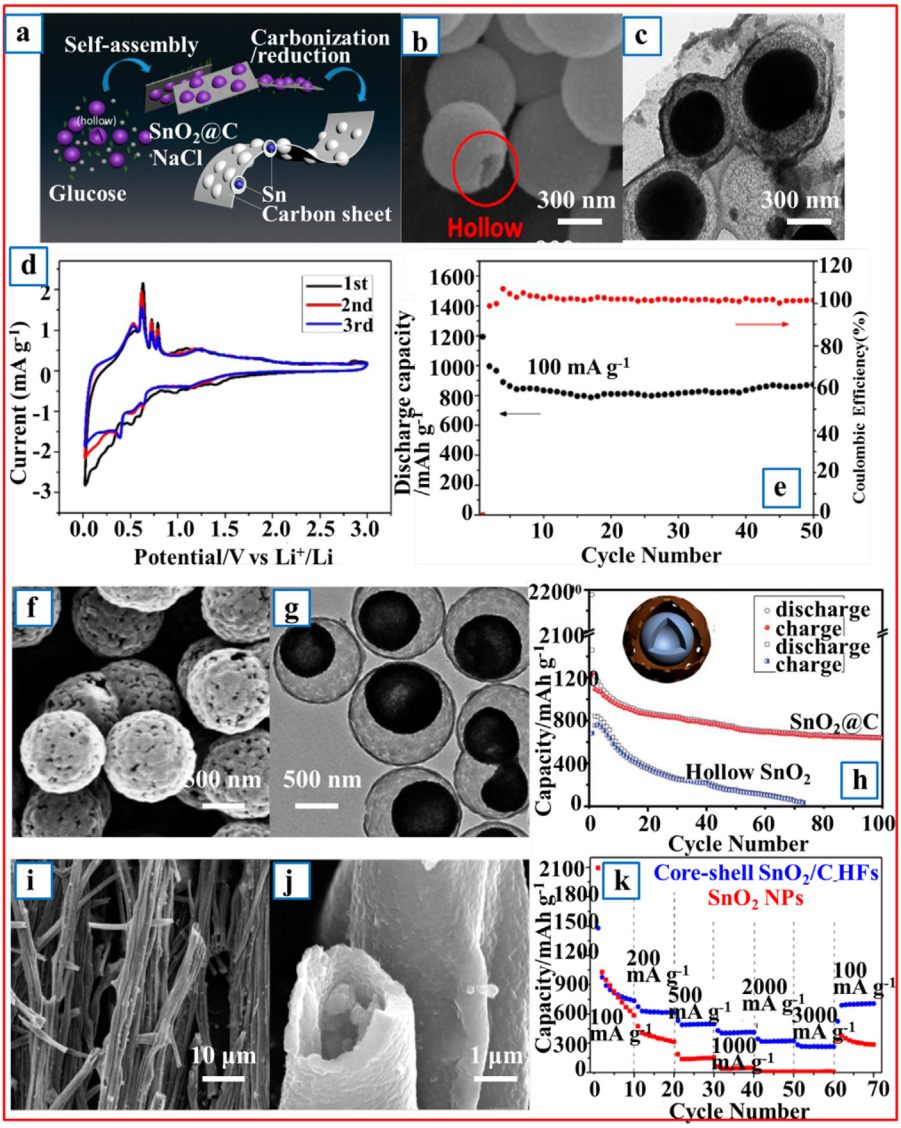

Fig. 5. (a) Synthetic procedure of SCE, (b) SEM images of hollow SnO_2 precursors and (c) TEM images of SCE, (d) CV curves at a scan rate of 0.1 mV s^{-1} in 0.02-3 V, (e) cycling performance of SCE at 100 mA g^{-1}. Adapted from ref. [173]. Copyright (2016) American Chemical Society. (f) FESEM and (g) TEM images of the SnO_2@C yolk-shell nanospheres, (h) cycling performance of the pure hollow SnO_2 particles and SnO_2@C yolk-shell nanospheres, (i) FESEM images and (j) TEM images of the core-shell SnO_2/C hollow fibers, (k) rate capability of bare SnO_2 nanoparticles and core-shell SnO_2/C hollow fibers at various current densities. Adapted from ref. [178, 179]. Copyright (2015) American Chemical Society; Copyright (2014) The Royal Society of Chemistry, respectively.

solvothermal strategy. Then, it was homogeneously dispersed in glucose/NaCl solution because NaCl is a thermally stable template. The SnO_2@C was reduced to Sn@C and the glucose was turned into carbon after carbonization process in Ar/H_2. The Sn@C yolk-shell structure could be clearly observed in Fig. 5b and c. The electrochemical test was used to evaluate the SCE electrodes at 0.1 mV s^{-1} (0.02–3 V) (Fig. 5d). The generation of solid electrolyte interface films resulted in the difference between the second and first cycles. This novel nano-architecture showed good electrochemical performance in LIBs. The electrodes still retained a capacity of 850 mAh g^{-1} after 50 cycles with initial capacity of 1200 mAh g^{-1}, which is higher than the traditional graphitic anode (373 mAh g^{-1}) (Fig. 5e). More efforts recently have been directed toward developing advanced core-shell structured nanomaterials and techniques to enhance the performance of electrode materials [174–177].

2.2.3. Other metal oxides with carbon shells

The process of Li storage in metal oxides consists of the decomposition and formation of Li_2O, along with the oxidation and reduction of metal particles; this process is different from the traditional Li deinsertion/insertion or Li-alloying/dealloying processes. However, these obstacles, including the low coulombic efficiency , large volume change and poor electronic conductivity during charge/discharge processes, limit their wide applications. Construction of a core-shell structure is regarded as an effective method for electrochemical performance improvement because it has the advantages of shortening the distance of Li^+ transfer, increasing electronic conductivity and buffering volume expansion. Huang et al. [180] introduced a two-step strategy to synthesize Fe_3O_4@C nanoparticles and this composite exhibited stable discharge capacity (800 mAh g^{-1}) with no significantly decrease after 100 cycles, which is much higher than the theoretical discharge ability of the commercial graphite. Following this line of thought, Li's group synthesized Fe_3O_4@C chains, rings, and spheres with adjustable magnetic properties by regulating time and temperature [181]. The results revealed that the Fe_3O_4@C chains (1410 mAh g^{-1}) and rings (1381 mAh g^{-1}) had superior cycling stability and better reversible capacity than monodisperse Fe_3O_4@C spheres (1031 mAh g^{-1}) because the closed ring and chains structure could distinctly enhance the ionic and electronic conductivity. Another advanced strategy to limit volume change is a reasonable combination of different structures, such as combining the Fe_3O_4@C with the nanotubes structure. The results indicated that the novel composite possessed high voids and large surface area. It also provided evidence supporting the conclusion that the carbon coating could enhance the electrode materials performance for LIBs. Fe_3O_4 composites have high electronic conductivity, similar to amorphous carbon. Therefore, they would be the most potential active materials, due to the higher tap densities, superior coulombic efficiencies.

SnO_2 is also regarded as a potential candidate for application in advanced materials, such as the next generation of lithium-ion batteries, due to the high theoretical capacity. Several SnO_2@C nanocomposites have been successfully prepared and recently exhibited excellent electrochemical performance [178,179,182–184]. For example, Wang et al. [178] synthesized uniform yolk-shell SnO_2@C nanospheres as the anode materials for lithium-ion batteries. This nanocomposite had uniform spherical morphology (Fig. 5f) and possessed a yolk-shell structure (Fig. 5g). This nanocomposite with a hollow highly crystalline SnO_2 core possessed high surface area (~205 m^2 g^{-1}), with large pore volume (~0.25 cm^3 g^{-1}). It also exhibited a high Li^+ storage capability (2190 mAh g^{-1}), good rate capability and excellent cycling stability. This novel nanocomposite improved the cycling performance with a reversible capacity of 630 mAh g^{-1} after 100 cycles (Fig. 5h). Some studies have also indicated that a hollow SnO_2@C sphere can shorten the pathway of Li^+ transportation, retard the volume expansion and improve the rate capability. Zhou et al. [179] prepared novel hollow SnO_2@C nanoparticles through coaxial electrospinning and used those nanoparticles as anode materials for lithium batteries. These nanocomposites presented hollow tubular fibers with an approximately 50–100 nm shell and average diameter of 2 μm (Fig. 5i-j). The existence of core-shell structure significantly improved rate capability than bare SnO_2 nanoparticles at various current densities (Fig. 5k). Meanwhile, this composite showed a high reversible capacity (1002 mAh g^{-1}), a high cycling stability and superior rate capability (remain 833 mAh g^{-1} over 500 cycles). The unique hollow core-shell structure can retard the volume expansion and contraction of electrode materials by providing sufficient voids during delithiation/lithiation processes. All results confirmed that the existence of carbon shell could significantly improve the performance of SnO_2 electrode materials, particularly when combined with mesoporous and hollow structures. TiO_2 composites are also a type of special electrode material due to the small volume change, excellent rate capability and high stability. Moreover, compared to $Li_4Ti_5O_{12}$ (1.9 V vs Li^+/Li), TiO_2 composites possess lower voltage (1.5 V vs Li^+/Li). However, the inherent low conductivity restricts their wide applications, thus combining with other highly conductive composites with core-shell structure is an effective strategy.

Other MOs have been widely studied in depth as the anode materials for lithium-ion batteries, except for the aforementioned Fe_3O_4, TiO_2, and SnO_2. However, most of the MOs cannot be coated with a carbon shell because many high valence metal elements can be reduced by a CO or H_2 atmosphere [185]. For example, Fe_2O_3, MnO_2, Co_3O_4, CuO, and MoO_3 can be reduced to Fe_3O_4, MnO, CoO, Cu_2O, and MoO_2 in turn, and the high temperature can also promote the generation of counterpart high valence metals. To obtain advanced core-shell nanostructure MOs materials with environment friendliness, low cost, superior energy density, and good mechanical stability for LIBs applications, various synthetic methods have been studied, such as the optimization of crystal structure of MOs materials, combination with MOs and active/inactive materials, and formation of nanoscale MOs materials. In particular, the reaction time and atmosphere need reasonable control to avoid the high valence metals being reduced. Correspondingly, some promising prospects can be inspired by previous reports, which can guide the direction of future research. Thus, more studies that focus on studying advanced core-shell structured nanomaterials and exploring the modification mechanism should be performed. Finally, new industrial techniques and large-scale production are the two key factors for nanomaterials in the practical application. We can also see the performance of Li-ion batteries with different types of core-shell structured nanomaterials in Table 2.

2.3. Core-shell structured nanomaterials applied to hydrogen storage

The utilization of H_2 as a carrier or energy source, such as fuel cell powered electrical vehicles, is restricted by the lacking of safe and effective H_2 storage system. In this section, we review the progress of various core-shell structured nanomaterials adsorbents for H_2 storage, including carbon materials, MOFs (metal organic frameworks), *etc*. The new techniques to improve the capacity of hydrogen storage are discussed, along with future directions. Since Dillon and co-workers first published their report on H_2 storage in carbon materials [202], increasingly more researchers have focused on H_2 storage in carbon materials. However, there are still some problems with the large-scale application of carbon materials to storage H_2 because carbon material is difficult to restore its re-adsorption capacity. Meanwhile, the impurities in the H_2 and carbon samples, the differences in accurate measurement, and the obscure mechanism of hydrogen adsorption are considered to be the causes of this difference in the H_2 storage capacities of carbon materials [203–206]. Recent studies have demonstrated that the core-shell nanostructure with carbon materials could significantly improve H_2 storage capacity. For example, Chang et al. [207] prepared CNF@Co and CNT@Co nanoparticles, and these nanocomposites exhibited excellent H_2 storage reversibility and superior H_2 storage capacity. The as-obtained CNF@Co and CNT@Co have high H_2 storage capacities of 739.4 mAh g^{-1} and 717.3 mAh g^{-1}, respectively, under ambient pressure and room temperature. They also found that the hydrogen storage capacity

Table 2
Summary of the performances of core-shell structured nanocomposites anode for lithium battery (reported in the literature since 2011).

Type	Active material	Surface area ($m^2\ g^{-1}$)	Synthetic method	CD[a]	DC[b] (mAh g^{-1}) (cycle 1)	CP[c]		Ref
						Cycle no.	DC[b] (mAh g^{-1})	
Lithium transition metal oxide	$Li_4Ti_5O_{12}$@Carbon	79	Solid-state reaction	1 C	153	1000	145 (10 C)	[186]
	$LiFePO_4$@CNT nanowires	34.3	Sol-gel route+ solid state reaction	17 mA g^{-1}	160	100	34 (0.2 C)	[187]
	$LiFePO_4$@CNT nanowires	72.9	Liquid deposition+ solvothermal	0.2 C	132.8	300	62.4 (20 C)	[188]
	F-doped $LiFePO_4$@C composite	–	Sol-gel+ heat treat	0.1 C	162	400	67	[189]
	$Li_3V_2(PO_4)_3$@C	130.8	Hydrothermal+ sol-gel method	5 C	138	1000	119	[158]
	$LiFe_{1/3}Mn_{1/3}Co_{1/3}PO_4$/carbon	–	Microwave heating rout	0.1 C	160	30	76 (20 C)	[190]
Si, Sn and alloys with carbon shells	Si/CNT encased in carbon	–	Electrospinning+ carbonization	C/10	1500	100	1000 (1 C)	[191]
	Core-shell amorphous Si@C nanoparticles	176	Laser-driven chemical vapor pyrolysis	2 C	800	500	1250 (0.2 C)	[192]
	Si/hollow carbon composite fibers	191	Coaxial electrospinning	0.2 A g^{-1}	903	100	804	[193]
	Mesoporous silica encapsulated by carbon core and shell	506	Hydrothermal+ calcination	500 mA g^{-1}	1055	150	1055	[194]
	Si@TiO_{2-x}/Carbon mesoporous microfiber composite	163	Hydrothermal+ Electrospinning+ Heat-treated	12 C	939	50	945 (0.2 C)	[195]
Other metal oxides with carbon shells	GeO_2/nitrogen-doped porous carbon	86.8	Sol-gel+ calcination	20 C	412	200	831 (0.5 C)	[196]
	Zn/$ZnFe_2O_4$@C mesoporous nanospheres	80	Sol-gel+ calcination	100 mA g^{-1}	1170	500	718	[197]
	Graphene@Fe_3O_4@C	136	Solvothermal	100 mA g^{-1}	1468	100	1200 (0.2 C)	[198]
	Core-shell structure Co_3O_4/CNF	331.8	Electrophoretic deposition+ annealing	200 mA g^{-1}	1446	50	911	[199]
	MnO@C hybrid	69.3	Hydrothermal+ calcination	0.3 A g^{-1}	691	200	934	[200]
	MnO@N-C	114	Hydrothermal+ carbonization	100 mA g^{-1}	799	60	578	[201]

[a] Current Density (CD).
[b] Discharge Capacity (DC).
[c] Cycling Performance (CP).

was much higher than the capacities of individual CNF (49.0 mAh g^{-1}) and CNT (29.9 mAh g^{-1}). Bao et al. [208] also synthesized C_{60}@Co nanocomposites, and these nanomaterials obtained high H_2 storage capacities of 907 mAh g^{-1} and superior cycle reversibility of H_2 storage under room temperature and ambient pressure.

Metal hybrids have been investigated intensively over four decades [209]. However, core-shell nanostructure metal materials are just starting to be used in electrochemical hydrogen storage [210]. Recently, Konda et al. [211] synthesized the Cd@Pd nanomaterial for H_2 adsorption and storage. When the molar ratio of Cd to Pd was 1:2, the prepared Cd@Pd nanomaterial showed the highest H_2 storage capacity among all materials. Moreover, a 340% increase compared with pure Pd nanoparticles of hydrogen storage could be achieved. Christian et al. [212] synthesized core-shell nanostructure $NaBH_4$@Ni using an antisolvent precipitation method. The storage capacity of $NaBH_4$@Ni was found to be of 5 mass %, and hydrogen kinetics were rapid during 5 cycles in less than 60 min. In recent years, core-shell structured nanomaterials have been developing swiftly in the sphere of H_2 storage due to their high H_2 storage capacity. There is still an enormous obstacle for the large-scale practical application of core-shell structured nanomaterials, because of their high reactivity and the melting of the related complex hydride.

3. Core-shell structured nanomaterials applied to energy conversion

3.1. Core-shell structured nanomaterials for solar cells

The radiant energy that the earth surface receives from the sun in one day is comparable to that humanity used in ten years. [213]. If we can translate this power into a source of energy that human beings can use directly, then the energy crisis that has long perplex society and the environmental pollution issues caused by fossil fuel burning will be efficiently solved. It will be a great step if chemical or other forms of energy could be obtained directly in a cost-free and efficient manner from solar energy. Therefore, many researchers have been devoting their attention to developing the devices and materials for the conversion of solar energy to chemical energy by solar cells. In particular, semiconductor core-shell nanocomposites are considered to be extremely promising materials due to their significantly improved photochemical stability. The inorganic shell materials are grown on the surface of a core quantum dots and it can enhance the surface passivation of the core quantum dots in the quantum dots solar cells. The inorganic shell is also expected to act as a barrier to offer a robust protection to the core quantum dots in the quantum dots solar cells. Moreover, both electronic and optical properties can be designed based on the surface electronic structure of the core materials and shell materials, but these requirements can't be achieved by simple single-function materials. The complex heterostructure, especially the bimetallic core-shell nanostructure composites, can greatly improve their intrinsic properties and produce new unique properties. To reduce the costs, it is an advisable strategy to replace the core of solid precious metal with a non-noble metal. Furthermore, it is also expected that the synergistic effect can be enhanced and take place when the shell is confined to a few single metal atoms. Besides, other properties may emerge by a few specific materials. Therefore, it is critical to expand the scope of core-shell materials and to further improve our controllable synthesis capability.

3.1.1. Dye-sensitized solar cells

Core-shell structured nanomaterials are ideal materials for light harvesting through multiple light reflections and scattering. Meanwhile, the working electrode of dye-sensitized solar cells (DSSCs) prepared by core-shell structured nanomaterials can adsorb considerable dyes; this ability is conducive to enhancing the efficiency of light conversion because the core-shell structure can enhance the light absorption ability of the core material by changing the chemical and physical properties, leading to high light conversion efficiency. To date, the electrode

materials of DSSCs with core-shell structure, which are widely studied, include TiO_2, ZnO and other composites because they are easily prepared.

TiO_2 is currently a common photocatalyst, and tremendous efforts have been made to enhance its activity. [214,215]. Mahmood et al. [216] synthesized WO_3@TiO_2 nanoparticles to improve the power conversion efficiencies (PCE) (11.2%). Dong et al. [51] prepared plasmonic silver nanowires@TiO_2 core-shell nanocomposites (AgNW@TiO_2), and the composites possessed high aspect ratio with several micrometers length, the diameter of shell is approximately 300 nm and diameter of core is 60–80 nm. The results of electrochemical analysis and electrical properties revealed that the AgNW@TiO_2 significantly facilitated electron-hole pairs separation, and then enhanced the charge collection productivity of DSSCs. In particular, the PCE (8.84%) was better than that of free-modified DSSCs (6.16%). It is expected to be a promising metal-modified technology to improve the energy conversion efficiency of DSSCs. Pang et al. [217] prepared hierarchical microspheres constructed from a SnO_2 shell and a TiO_2 core using a one-step solvothermal method. They found that the content of precursor Sn^{4+} had a great influence in the formation of the hierarchical microspheres. The TiO_2@SnO_2 composites showed higher power conversion efficiency because the hierarchical structure of the microspheres and large surface area can lead to light scattering, a suppression of charge recombination, and an increase of dye adsorption as well as prolonging the electron lifetime. To further improve the PCE of DSSCs, Qi et al. [218] found that localized surface plasmons (LSPs) can improve the adsorption ability of the materials to dye molecules; this outcome is conducive to enhance electron collection and improve the performance of device. For example, the PCE of Ag@TiO_2 nanoparticles increased from 7.8% to 9.0% after LSPs. Meanwhile, Liu et al. [219] studied the effect of the thickness of shell to PCE and found that Au@TiO_2 nanoparticles with 5 nm thick shell exhibited the maximum efficiency enhancement (23%) in DSSCs after LSPs.

Hybrid materials of zinc oxide and titanium dioxide used for the DSSCs have also attracted much attention. Lin et al. [220] prepared ZnO@TiO_2 nanowires and used them as the photoanodes for DSSCs. ZnO nanowires were synthesized on an FTO glass through chemical bath deposition, and then the surface of ZnO nanowires were precisely enwrapped with a layer of TiO_2 to enhance the chemical stability of ZnO. A higher PCE was obtained for the ZnO@TiO_2 nanowires based DSSC with optimized dye sensitization time than for the pristine ZnO nanowires (0.75%). The high performance could be attributed to the TiO_2 shell, which could act not only as a protective layer to avoid the generation of Zn^{2+}/dye complexes on the surface of ZnO nanowires but also as a barrier against the recombination of injected electrons at the interface of ZnO nanowires and the electrolyte. Chen et al. [221] prepared ZnO@ZnS nanowire arrays as photoanodes for efficient DSSCs, and these composites exhibited enlarged surface area and excellent light-scattering effect. The DSSCs obtained the high efficiency (2.09%). The improvement of efficiency was 140%, which was higher than other cells without a shell. In addition, the ZnO core can accelerate the rate of electron transfer. The ZnS shell can impede the recombination of the electrolyte and injected electrons. Samsuri et al. [222] investigated the performance of TiO_2@ZnO DSSC. They found that the device exhibited high conversion efficiency (η) (0.622%) with the J_{sc} of 1.89 mA cm^{-2}, V_{oc} of 0.64 V and FF of 0.51 (photovoltaic parameters: J_{sc}-the short-circuit current density, V_{oc}-the open-circuit voltage, and FF-the fill factor; PCE = $J_{sc} \times V_{oc} \times$ FF). To further improve the performance of TiO_2/ZnO, Song et al. [223] prepared TiO_2@ZnO rice grains through coaxial electrospinning and calcination. Using this original structure as the photoanodic material, the DSSCs had high η (5.31%), which increased by 23.9%, based on the TiO_2 rice grains. This increase was primarily ascribed to the improvement in both electron collection efficiency and light harvesting efficiency, and the effective suppression of charge recombination.

3.1.2. Quantum dot solar cells

Due to their distinctive characteristics, including low cost, simplicity in fabrication, *etc*., quantum dot-sensitized solar cells (QD-SSCs) are famous energy devices. However, the PCE of many QDSSCs is weaker than those of DSSCs. The maximum PCE can only reach 12% because the finite adsorption ranges and electron recombination were produced at the electrolyte interfaces. Therefore, novel sensitizers are needed to develop for improving the η of QDSSCs. Core-shell structured nanomaterials are suitable for photosensitization due to the unique core-shell structure and high emission and adsorption spectra. Various core-shell structured nanomaterials, including CdS, [224] PbS, [225,226] CdTe, [227] ZnSe, [228] and Ag_2S, [229] *etc*, have been investigated in QDSSCs. Wang et al. [230] fabricated highly efficient CdTe@CdSe QD-SSCs through the covalent bonding of a molecule mercaptopropionic acid-capped QD sensitized around TiO_2 mesoporous film electrodes. The corresponding photographs and absorption spectra of the CdTe@CdSe and CdSe are shown in Fig. 6a. The high absorbance of the CdTe@CdSe film reflected the high-loading amount of the QDs, resulting in the deep color of the film electrodes. The *J-V* curves of the reference CdSe and CdTe@CdSe cells suggested that the CdTe@CdSe QD-based cells had good photovoltaic performance and chemical stability (Fig. 6b). Meanwhile, the intensity-modulated photocurrent (IMPS) results indicated that the τ_d for the CdTe@CdSe cells (1.1–5.9 ms) was significantly shorter than those reference CdSe solar cells (2.3–13.2 ms) (Fig. 6c), resulting in larger charge formation in the CdTe@CdSe cells, creating an enhanced electron concentration in the substrate. It also exhibited a record PCE of 6.76% (V_{oc} = 0.606 V, J_{sc} = 19.56 mA cm^{-2}, and FF = 0.569).Yang et al. [231] chose $CdSe_{0.65}Te_{0.35}$ as a model core material, and a CdS shell was then coated around the $CdSe_{0.65}Te_{0.35}$ core QD to decrease the surface defect density and improve the stability of the core QDs. The PCE of the $CdSe_{0.65}Te_{0.35}$ QDSSCs was increased by 13% compared to that of plain $CdSe_{0.65}Te_{0.35}$ QDSSCs by optimizing the thickness of CdS shell. With the further overcoating of SiO_2 and a-TiO_2 barrier layers around the QD-sensitized photoanode, the PCE of champion CdSeTe QDSSCs reached 9.48% (V_{oc} = 0.713 V, J_{sc} = 20.82 mA cm^{-2}, FF = 0.639) with average PCE 9.39 ± 0.09% under AM 1.5 G one full sun illumination (Fig. 6d-f). This system could also offer a fast charge separation and low charge recombination rate. Searching suitable QD sensitizers to amplify the light-harvesting range, retarding charge recombination, and accelerating charge separation are effective methods of improving PCE of QDSSCs. The Ag_2S QD exhibits negligible toxicity and has tunable bandgap energy (E_g) of approximately 1.1 eV that is close to the perfect E_g of ~1.13 eV, making it a potential modular for construction of high performance photovoltaic device [232]. Meanwhile, ZnO has been attracting extensive attention over the past decade. ZnO exhibits a similar conduction band edge (−4.36 eV *vs.* −4.41 eV of TiO_2), with a high charge mobility (130–200 cm^2 V^{-1} S^{-1} *vs.* 0.1–4 cm^2 V^{-1} $S^{-1}$of TiO_2), which is beneficial to efficient charge transport, with less recombination [233]. Zhang et al. [229] synthesized the environmental-friendly 2D ZnO@Ag_2S nanowire arrays as electron transporters and light absorbers. Compared to the device with Ag_2S QD, the device with a core-shell ZnO@Ag_2S photoanode exhibited a higher PCE and increased by 32%. The improved PCE was principally because the ZnO enhanced the ability to collect photogenerated electrons and accelerated the electrons transfer rate from the QD to contact.

3.1.3. Silicon/organic solar cells

Silicon nanowires have been used as an the energy storage device [234], energy chains or energy harvesting devices (similar to thermal electrical generators) [235,236], and most importantly, as solar cells [237,238]. In 2007, the first silicon single nanowire solar cells were fabricated with the maximum output power of 200 pW and conversion efficiency of 3.4%. They exhibited the possibility of this kind of compact photovoltaic cells to be used as the integrated power source for opto-electronic nanosystems. [239] Then, Si-based core-shell structured nanomaterials have attracted more attention. Adachi et al. [240] synthesized core-shell structure silicon-based solar cells, and this device exhibited different electrochemical performance with different Si shell.

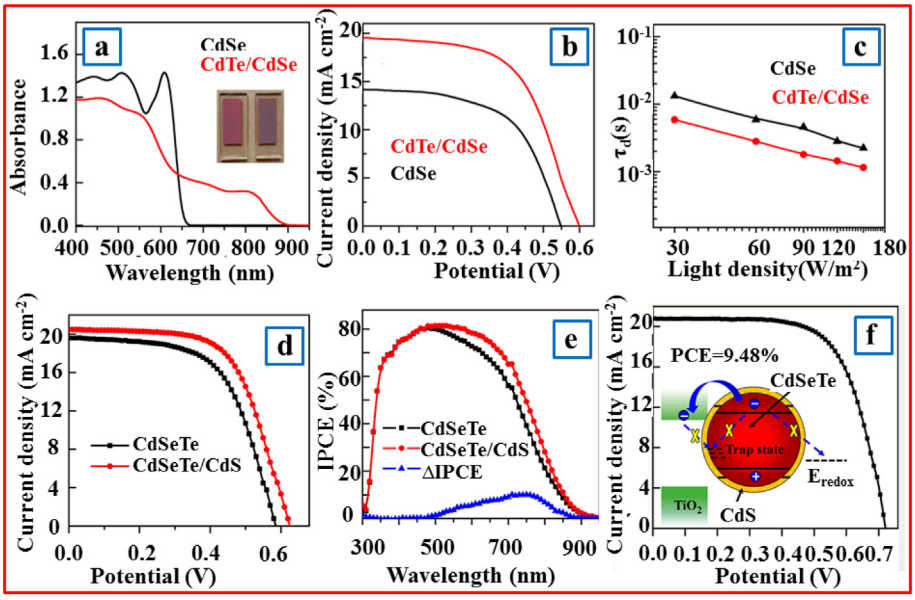

Fig. 6. (a) Diffuse reflectance absorption spectra of identically sized CdSe QD-sensitized TiO_2 film and CdTe/CdSe electrodes, (b) *J-V* curves, (c) electron lifetime; (d) *J-V* curves of CdSeTe@CdS (red) and CdSeTe (black) representative cells under the irradiation of 1 full sun, (e) incident photon to current efficiency curves, and (f) the schematic illustration of the proposed electron transfer mechanism. Adapted from ref. [230,231]. Copyright (2013) American Chemical Society; Copyright (2015) American Chemical Society, respectively. (For interpretation of the references to colour in this figure legend, the reader is referred to the web version of this article.)

The enhancement of short circuit current was 26% or 15% when using a nanocrystalline or an amorphous Si shell, respectively. Compared to the planar device (12.1 mA cm^2), the core-shell structure Si-based device with amorphous Si shell showed a higher J_{sc} (13.9 mA cm^2). Beak et al. [241] prepared an ultrathin and low cost solar cell based on $Cd_{0.5}Zn_{0.5}S$@ZnS quantum dots. These flexible ultrathin solar cells only had ~30 μm thickness and possessed flexible stable and twistable characteristics. The unique core-shell structure improved the power conversion efficiencies by 0.7% through an energy downshift effect and improved external quantum productivity in the ultraviolet light area. Furthermore, the devices showed superior bending fatigue properties and PCE, with cycle stability maintained at ~12.4% after 5000 cycles.

Low-cost and high-efficiency organic solar cells have attracted much attention. Multifarious metal nanocomposites have also been investigated in organic solar cells to improve PCE [242–244]. Liu et al. [245] prepared the Au@Ag nanocuboids for organic solar cells. These nanocomposites exhibited stronger broadband plasmonic that could be adjusted to match the optical light absorption spectroscopy by tuning the thickness of Ag shell. Researchers also found that the PCE of the organic solar cells enhanced for up to 22.8% under optimum conditions. Meanwhile, Baek et al. [246] coated the surface of Au core with a thin Ag shell to prepare Au@Ag nanocube as a scattering enhancer. This core-shell composite exhibited stronger scattering efficiency. Meanwhile, other core-shell structured nanomaterials have also been reported, such as Au@SiO_2 [247], SnO_2@TiO_2 [248], CdSe/PbS core-shell nanotetrapods [249], and Ag@organic (organic = PVA, 2-nitroaniline, PVP and 4-choloroaniline) [250]. The electrochemical performance of solar cells with different core-shell structured nanomaterials is shown in Table 3.

3.2. Core-shell structured nanomaterials for fuel cells

Fuel cells (FCs) have attracted more attention and development due to their low emissions and high PCE. The catalyst plays a significant role in FCs. For example, the catalyst on the anode can oxidize the fuel to form protons which are conducted across the electrolyte to the cathode. The catalyst on the cathode can reduce oxygen to form oxygen ions, and then oxygen ions combine with the protons to produce water. However, the catalysts currently used still face many problems, such as low stability and high costs. It is important to exploit low-cost electrocatalysts with highly enhanced kinetics. Core-shell nanostructured materials can significantly reduce the loading of noble metals in electrocatalysts for FCs. They have the potential to obtain high performance catalysts with improved durability and catalytic activity compared to the commercial Pt/C electrocatalysts. Furthermore, a wide array of transition metal (TM) elements have been studied and incorporated into TM/Pt core-shell composites. In general, TMs such as Ti, Cr and Sc are usually used as the shell materials because these elements are easily being oxidized and electro-negativities. However, this will decrease the stability of these systems. Therefore, it is wise to adopt appropriate synthetic method to optimize the core-shell structure to solve this problem. Optimizing the shell thickness is one of the most common methods. While some studies proved that the catalysts with thin or monolayer Pt shell were most active, [274] and other researchers found higher activities for catalysts with slightly thicker shells. [275] Another strategy or requirement may focus on improving active site availability and surface area of catalysts. Core-shell structured nanomaterials can improve the stability and activity of the catalyst and offer special light, electric, and magnetic properties due to the unique core-shell structure. There are many types of FCs. The lower temperature fuel cells, including polymer electrolyte membrane FCs (PEMFCs), alkaline FCs, and phosphoric acid FCs (PAFCs), *etc.*, essentially operate on H_2 fuel. For the higher temperature FCs, including solid oxide FCs (SOFCs) and molten carbonate FCs, can also electrochemically oxidize CO. Core-shell structured nanomaterials have been widely used in the design of high current density and high efficiency FCs because the construction of fuel cells requires cathodes and anodes to accelerate the diffusion of the chemical wastes produced and fuel. Here we only discuss the application of the core-shell structured nanomaterials in the two promising SOFCs and PEMFCs technologies.

3.2.1. PEMFCs with noble metals

Generally, core-shell structured materials for electrodes in FCs play two roles. One is transporting gases from/to the FCs electrode. The crucial component of PEMFCs is the membrane electrode assembly (MEA) which is made up of a catalyst layers, polymer electrolyte membrane for the cathode and anode, and GDLs (gas diffusion layers). In PEMFCs, the core-shell structured nanomaterials play a critical role in improving

Table 3
Summary of the performances of core-shell structured nanocomposites anode for solar cells (reported in the literature since 2011).

Type	Active material	Synthesis method	J_{SC}(mA cm^{-2})	V_{OC} (V)	PCE (%)	FF (%)	Thickness	Ref
Dye-sensitized solar cells	Ag@TiO_2 NPs	Spin coating	8.31	0.60	9.0	67	1.5 μm	[251]
	SnO_2@TiO_2	Electrospinning + direct sintering + deposit	14.71	0.723	5.11	48	13 μm	[252]
	TiO_2@SnO_2	Solvothermal	12.55	0.756	6.24	66	11.4 μm	[253]
	Core-shell TiO_2 microspheres	Solvothermal	18.6	0.664	8.22	65	12 μm	[254]
	Hierarchical core-shell TiO_2	Solvothermal	17.22	0.745	8.90	69	21.6 μm	[255]
	SiO_2/TiO_2 core-shell NPs	Sol-gel	15.9	0.71	7.9	70	10 μm	[256]
	Au@TiO_2 NPs	Solvothrmal+ plasmonic heating	14.73 ± 0.65	0.71 ± 0.01	7.38 ± 0.31	70 ± 1	10 μm	[219]
	TiO_2-ZnO core-shell rice grain	Coaxial electrospinning +calcination	11.5	0.783	5.31	59	8 μm	[257]
	Ag@SiO_2	Solvothermal	14.4	0.70	8.4	73.5	4.474 μm	[258]
	Core-shell structure β-$NaYF_4$: Yb,Er@SiO_2@Au	Stöber sol–gel process	15.84	0.80	8.23	65.72	7.5 μm	[259]
	Au@SiO_2 core-shell NPs	Spin-coating +thermally evaporated	3.37	0.7466	1.95	67.0	1 μm	[260]
Quantum dot solar cells	core-shell PbS/CdS	Hydrothermal + cation exchange +hot injection technique	21.3	0.475	4.16	41	170 nm	[261]
	PdS/CdS core-shell quantum dots and TiO_2 nanorod arrays	Hydrothermal+ wet chemical synthesize	17.38	0.515	4.43	50	–	[262]
	ZnO/PbS core/shell nanorod arrays	Successive screen-printing+ chemical bath deposition+ thermal deposition	11.17	0.52	3.06	52.68	11 μm	[263]
	Quasi core-shel PbS/graphene quantum dots	Hot injection method	12.3 ± 1.2	0.59 ± 0.04	4.1 ± 0.2	56 ± 3	360 nm	[264]
	Type-I core-shell CdSeTe/CdS	Successive screen-printing+ ex-situ ligand exchange	20.50	0.626	8.02	61.9	16 μm	[265]
	Core-shell ZnTe/CdSe	Successive screen-printing+ deposition	19.65	0.642	7.17	57	6 μm	[266]
	Core-shell $Cd_{0.5}Zn_{0.5}S$/ZnS	Hydrothermal+ thermal evaporator	33.05	0.495	12.37	75.63	30 μm	[267]
Silicon solar cells	Multiple core-shell structure TCO/Al_2O_3/a-Si: H(P^++i)/c-Si nanowire	Atomic layer deposition	23.13	0.532	9.93	80.7	–	[268]
	Core-shell structures Si nanowire	Wet etching technique+ chemical vapor deposition	29.27 ± 0.44	0.53 ± 0.01	12.43 ± 0.33	81.05 ± 5.2	5 μm	[269]
Organic solar cells	Core-shell Au@Ag nanocubes	Hydrothermal	17.50	0.75	9.19	70	–	[270]
	Core-shell Au/Ag nanocuboids	Hydrothermal	19.39	0.792	10.59	69.1	–	[271]
	$SmPO_4$@Ei^{3+}-doped SiO_2 compoiste	Sol-gel+ hydrothermal+ precipitate+ spin-coating	7.97	0.727	3.30	57	250 nm	[272]
	Core-shell PbSe/PbS	Schlenk line techniques+ deposition	11.8	0.46	6.5	49	250 nm	[273]

electrode kinetics and minimizing losses, and noble metals are still regarded as being the best electrocatalysts for PEMFCs up to today.

Noble metals are valued for their excellent activity, selectivity and stability. Among them Pt-based catalysts are a kind of promising materials for hydrogen and methanol oxidation due to their high catalytic activity and ideal chemical inertness [276–278]. For instance, Chai et al. [279] synthesized carbon spheres with mesoporous shell and hollow structures. The carbon spheres were used as a support material for Pt_{50}-Ru_{50} catalyst and exhibited much higher specific activity for methanol oxidation. The authors also demonstrated that the existence of carbon spheres could significantly improve the catalytic activity and electrochemical stability of the noble metal catalysts for methanol oxidation. Lin et al. [280] synthesized Co@Pt/C nanocomposite through two-step reduction and heat treatment in N_2 and H_2 mixture, and this catalyst exhibited much higher specific activity with a low content of Pt. The Co@Pt/C catalyst was used as the negative electrode of the PEMFCs and produced a high-power density (475 mW cm^{-2}/0.475 V) because the existence of core-shell structure is conducive to enhance the stability and the active surface area of catalyst. Due to the high cost of rare Pt, enormous amount of studies devoted to developing novel and high efficiency core-shell Pt-based catalyst with a minimum content of Pt [281–283]. Liu et al. synthesized Pt@Au nanorods with carbon supported and exhibited superior electrochemical performance via a wet chemical reduction strategy (Fig. 7a and b) [284]. The oxygen reduction reaction (ORR) kinetics exhibited that the PtAu shell catalyst showed higher stability than a pure Pt shell in 0.5 M H_2SO_4 before and after 50 cycles (defined as L) (Fig. 7c). Meanwhile, the experimental results of cyclic stability suggested that a huge loss of electrochemical surface area (ECSA) for the PtAu shell and Pt/C, indicating that the Pt shell is more electrochemically stable than its counterparts (Fig. 7d). It is also an effective method to synthesize bimetallic materials with core-shell structure formed by noble metal and transition metal. Rashid et al. [285] anchored Ag@Pt nanoparticles on the multiwall carbon nanotubes (MWNT) and applied to methanol fuel cells and electrochemical gas sensors. These composites also showed a higher peak point current than other comparable Pt/C or Pt-MWNT for methanol oxidation, and the results exhibited excellent stability and good detection times, with a high range of 5-1000 ppm. This enhanced performance contributed to the unique core-shell nanostructure, which provided an effective interactions and highly active surface between Ag and Pt.

Du et al. [286] synthesized the Pt@Cu intermetallic nanotubes that showed superior catalytic activity and rather high durability compared to the conventional Pt/C catalyst. The results demonstrated that the activity of Pt@Cu was 4 times higher than that of Pt/Cu, and the durability was 10 times higher than that of Pt/C. Yang et al. [287] synthesized Au-Pd bimetallic with a thin Pd shell and an Au core. This composite was used as the cathode catalysts in fuel cells and exhibited excellent stability and activity for ORR under a neutral condition. The strong lattice strain effect and electronic interaction between the Pd shell and Au core improved the electrochemical performance of the catalyst. Meanwhile, the thickness of the Pd shell also influences the performance of catalysts. Lee et al. [285] synthesized Ni@Pt nanoparticles with a controllable particle shape and thickness of the Pt shell, using a one-step reaction method. The electrochemical data.

3.2.2. Higher temperature SOFCs with transition metal/nonmetal oxides

Depending upon the FCs design, core-shell structured nanomaterials for PEMFCs and SOFCs can be prepared either for the cathode and anode material. In PEMFCs, porous core-shell structures can effectively reduce

of transport limitations, and it can significantly enhance the accessibility of the active sites by electrolyte and gas phase due to the presence of mesopores and large pores. In SOFCs, the unique structure can also provide sufficient porosity for GDLs to ensure effective reactant delivery. Core-shell structured nanomaterials with high surface area are quite important for cathode and anode materials because it can reduce the operating temperature of SOFCs through reducing the barrier for chemisorption and allowing easy diffusion of gaseous reactants.

It is advisable to reduce the Pt loading or use the non-noble metal catalysts in terms of cost, stability and sustainability. Therefore, developing higher temperature SOFCs with transition metal and nonmetal electrocatalysts with good ORR durability and high activity have become a popular research topic. Zhang et al. [289] prepared Ni/Al_2O_3 with a shell of MSU-1 and used them as the catalyst for SOFCs. This catalyst exhibited superior stable methane conversion and hydrogen yield in hydrogen evolution experiment. It is difficult to obtain the low cost and abundant ORR catalyst, thereby hindering the wide application in fuel cells. Heteroatom-doped carbon-based catalyst has recently attracted much more attention. Zhong et al. [288] synthesized B- and N-co-doped carbon-based catalyst (NB-CPs) and used it as the catalyst for SOFCs. This device obtained a high current density, which could be comparable to that of noble metal catalysts, such as Pt (Fig. 7e). The LSV results suggested that the higher rotation speeds would increase the limiting current density (Fig. 7f). This nanocomposite exhibited a high-power density (642 mW cm^{-2}) and higher cathode potential over current density (Fig. 7g and h). Note that the cathode potential decreases rapidly along with the increasing of current density for N-CPs and CPs cathodes. If it can be large batch preparation with low cost, the NB-CPs might be a promising substitutable cathode catalyst. In addition, Lim et al. [290] synthesized NiO@GDC nanoparticles with GDC shells and NiO cores. These composites were used as an anode catalyst and exhibited superior electrochemical performance. Due to the existence of the GDC shell, the performance of catalyst remained unchanged after 500 cycles. Lee et al. [291] synthesized Ni@YSZ (yttria stabilized zirconia) nanoparticles through hydrothermal technique. The YSZ nanoparticles were uniformly loaded on the surface of the Ni core and significantly improved the conductivity. Wu et al. [292] synthesized a novel samarium-doped ceria (SDC)@LiZn-oxide nanoparticle for SOFCs, in which the SDC were covered by a LiZn-oxide shell. Electrical property measurements demonstrated that the thin shell could greatly improve the ionic conductivity (0.1S cm^{-1}).

3.3. Core-shell structured nanomaterials for photocatalytic hydrogen production

There has been much concern that the use of solar energy and other renewable resources for the photocatalytic hydrogen production was regarded as a potential for environmental remediation and clean energy generation in the future. Theoretically speaking, an excellent photocatalyst for hydrogen production should have more positive valence band edge potential than $E(O_2/H_2O)$ (1.23 V at pH = 0) and a more negative conductive band edge potential than $E(H^+/H_2)$. There are many splendid reviews of various composites, such as TiO_2, CdS, $BiWO_3$, ZnS and g-C_3N_4, and structures for photocatalytic H_2 production [293–297]. Thus, we simply introduced the research progress of core-shell structured nanomaterials for photocatalytic H_2 production in recent years.

Efficient hydrogen production is regarded as a critical strategy to solve the future energy crisis. Sun et al. [298] synthesized CoP_x@CdS nanorods and demonstrated superior performance of photocatalytic H_2 production with visible light irradiation. The photocatalyst generated hydrogen with evolution rate of ~500 μmol h^{-1} mg^{-1}. The maximum hydrogen yield was ~35% in aqueous solution under optimal conditions and the turnover numbers achieved ~630,000 per mole Co (Fig. 8a-c). CdS is a photocatalyst with good light response for H_2 production, however, the rapid photocorrosion and recombination of photogenerated electron-hole pairs restrict its wide application. To solve these issues, Wang et al. [299] prepared PANI@CdS as the photocatalyst and studied the inhibition mechanism of photocorrosion. This photocatalyst, with a thin PANI shell, exhibited high H_2 production efficiency of 310 μmol h^{-1} in 30 h without deactivation (Fig. 8d-f) because the PANI possesses high-occupied molecular orbital and the photogenerated holes can effectively migrate from valance band of CdS to it. The results also revealed that the newly formed C-S or N-Cd bonds could inhibit sulfide ions to reduce the sulfur and then effectively inhibit the photocorrosion. Yan et al. [300] synthesized CdS@ZnO nanofibers through single cylinder electrospinning. The CdS@ZnO nanofibers exhibited superior photocatalytic efficiency and stability for H_2 production (Fig. 8g-i). Stability and efficiency of photocatalysts are essential to realize the practical applications of them for photocatalytic hydrogen production from industrial sulfide effluent. Kim et al. [301] synthesized $NiFe_2O_4$@TiO_2 magnetic nanoparticle and used it as a photocatalyst, resulting in

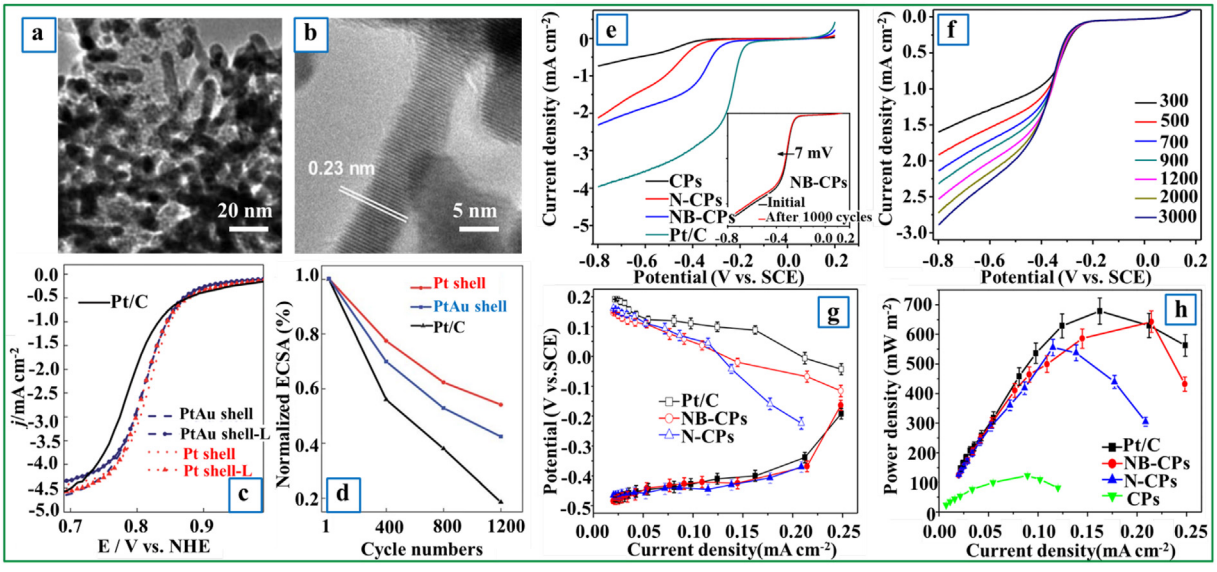

Fig. 7. (a) and (b) HRTEM images of the PtAu shell, (c) the LSV recorded in 0.5 M H_2SO_4 saturated with O_2 for the Pt/C catalysts and Pt-Au nanorods, (d) the normalized ECSA for the Pt/C catalysts and Pt-Au nanorods during 1200 potential cycles. Adapted from ref. [284]. Copyright (2012) The Royal Society of Chemistry. (e) Rotating-disk electrode LSV at 900 rpm (Inset: ORR polarization curve of NB-CPs before and after 1000 scanning cycles), (f) rotating-disk electrode LSV of NB-CPs at various rotation rates, (g) individual potential and (h) power density versus current density curves of the MFCs with various cathode catalysts. Adapted from ref. [288]. Copyright (2014) Elsevier B.V.

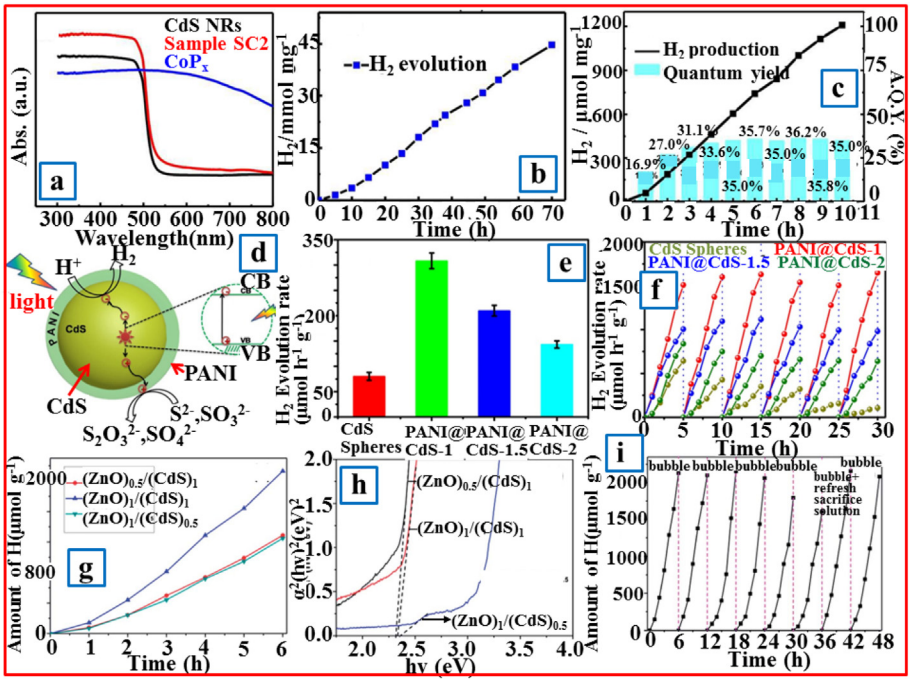

Fig. 8. (a) UV–vis diffuse reflectance spectra of CoP_x, SC2 sample and CdS NRs, (b) long-term H_2 evolution on SC2, (c) time courses of H_2 evolution and apparent quantum yield on SC2, (d) schematic illustrating the mechanism of CdS@PANI core-shell nanospheres for H_2 production under visible light irradiation, the photocatalytic H_2 production rates of PANI@CdS core-shell nanospheres and porous CdS nanospheres (e) volume histogram and (f) rate curves, (g) photocatalytic hydrogen production efficiency of $(CdS)_x/(ZnO)_y$, (h) plots of the band gap energy in direct transition recorded from the sample $(CdS)_x/(ZnO)_y$, (i) time course of photocatalytic H_2 production over sample $(CdS)_1/(ZnO)_1$. Adapted from ref. [298–300]. Copyright (2016) The Royal Society of Chemistry; Copyright (2016) Elsevier B.V.; Copyright (2013) The Royal Society of Chemistry.

significantly enhanced photocatalytic efficiency and stability. The results revealed that the H_2 production efficiency with the core-shell structured $NiFe_2O_4$@TiO_2 nanocatalyst was 10 times greater than that of either pure $NiFe_2O_4$ or TiO_2. Although various core-shell structured nanomaterials have been used for photocatalytic H_2 production, large scale use of core-shell structured nanomaterials still faces many challenges. Developing core-shell structured porous photocatalysts, particularly non-noble core-shell structured nanomaterials with N-doped, S-doped, graphene and g-C_3N_4 modification, would be an effective and promising strategy to improve the H_2 evolution performance.

4. Conclusion and perspectives

In this review, the important achievements of core-shell structured nanomaterials in energy storage and conversion are summarized. Meanwhile, the relationships among the unique core-shell structure, energy storage and conversion efficiency have also been investigated. However, it is found that computational chemical research on core-shell structures for energy applications are scarcely done. More attention should be paid to the fundamental studies of core-shell materials in the future review work. More theoretical studies can contribute to improve the synthesis process and experimental trials of novel core-shell nanomaterials, and to better understand the mechanisms in their application.

The physical property compatibility between the shell and core materials and their construction are rarely studied, but they are important factors to determine the stability of the whole structure. For instance, the differences in thermal expansion coefficients between the shell and core will lead to form alloys or poor adhesion. Thus, to enhance the quality of the core-shell nanomaterials is another focus in future research. The adoption of different elements for the shell and core respectively is beneficial to find the stable structure and to promote the generation of new core-shell nanomaterial, which will help to achieve the goal of sustainability. Finally, this review gives some special examples of the practical application of core-shell nanomaterials in energy conversion and storage. It is found that the practical application requires large-scale, low-cost, and high-yield fabrication methods of high-quality core-shell nanomaterials. The present advances in core-shell structured nanomaterials provide a solid base for the development of advanced green core-shell structured nanomaterials in the near future.

Acknowledgements

The study was financially supported by Projects 51579096, 51521006 and 51222805 supported by National Natural Science Foundation of China, the Key Research and Development Project of Hunan Province of China (2017SK2241), the National Innovative Talent Promotion Program of China (2017RA2088), the National Program for Support of Top–Notch Young Professionals of China (2012), and the Program for New Century Excellent Talents in University from the Ministry of Education of China (NCET–11–0129).

References

[1] Lai X, Halpert JE, Wang D. Recent advances in micro−/nano-structured hollow spheres for energy applications: from simple to complex systems. Energ Environ Sci 2012;5:5604–18.
[2] Hu J, Li M, Lv F, Yang M, Tao P, Tang Y. Heterogeneous $NiCo_2O_4$@polypyrrole core/sheath nanowire arrays on Ni foam for high performance supercapacitors. J Power Sources 2015;294:120–7.
[3] Zhou H, Li X, Fan T, Osterloh FE, Ding J, Sabio EM. Artificial inorganic leafs for efficient photochemical hydrogen production inspired by natural photosynthesis. Adv Mater 2010;22:951–6.
[4] Guo Z, Liu W, Su BL. Why so strong for the lotus leaf? Appl Phys Lett 2008;93:1.
[5] Geim AK, Novoselov KS. The rise of graphene. Nat Mater 2007;6:183–91.
[6] Georgakilas V, Otyepka M, Bourlinos AB, Chandra V, Kim N, Kemp KC. Functionalization of graphene: covalent and non-covalent approaches, derivatives and applications. Chem Rev 2012;112:6156–214.
[7] Pykal M, Šafářová K, Šišková KM, Jurečka P, Bourlinos AB, Zbořil R. Lipid enhanced exfoliation for production of graphene nanosheets. J Phys Chem C 2013;117:11800–3.
[8] Gawande MB, Bonifacio VDB, Varma RS, Nogueira ID, Bundaleski N, Ghumman CAA. ChemInform abstract: magnetically recyclable magnetite-ceria (nanocat-Fe-

Ce) nanocatalyst-applications in multicomponent reactions under benign conditions. Green Chem 2013;44:1226–31.
[9] Tang L, Wang J, Zeng G, Liu Y, Deng Y, Zhou Y. Enhanced photocatalytic degradation of norfloxacin in aqueous Bi2WO6 dispersions containing nonionic surfactant under visible light irradiation. J Hazard Mater 2016;306:295.
[10] Deng Y, Tang L, Zeng G, Zhu Z, Yan M, Zhou Y. Insight into highly efficient simultaneous photocatalytic removal of Cr(VI) and 2,4-diclorophenol under visible light irradiation by phosphorus doped porous ultrathin g-C_3N_4 nanosheets from aqueous media: Performance and reaction mechanism. Appl Catal B Environ 2017;203:343–54.
[11] Hou W, Yuan X, Yan W, Zeng G, Dong H, Chen X. In situ synthesis of In_2S_3 @MIL-125(Ti) core–shell microparticle for the removal of tetracycline from wastewater by integrated adsorption and visible-light-driven photocatalysis. Appl Catal B Environ 2016;186:19–29.
[12] Zeng HC. Integrated nanocatalysts. Accounts Chem Res 2013;46:226.
[13] Yang G, Tang L, Zeng G, Ye C, Tang J, Pang Y. Simultaneous removal of lead and phenol contamination from water by nitrogen-functionalized magnetic ordered mesoporous carbon. Chem Eng J 2015;259:854–64.
[14] Wittstock A, Zielasek V, Biener J, Friend CM, Bäumer M. Nanoporous gold catalysts for selective gas-phase oxidative coupling of methanol at low temperature. Science 2010;327:319.
[15] Silva R, Asefa T. Noble metal-free oxidative electrocatalysts: polyaniline and Co(II)-polyaniline nanostructures hosted in nanoporous silica. Adv Mater 2012;24:1878–83.
[16] Hu M, Furukawa S, Ohtani R, Sukegawa H, Nemoto Y, Reboul J. Synthesis of prussian blue nanoparticles with a hollow interior by controlled chemical etching. Angew Chem Ed Int 2012;51:984–8.
[17] Ren X, Zeng G, Tang L, Wang J, Wan J, Liu Y. Sorption, transport and biodegradation-An insight into bioavailability of persistent organic pollutants in soil. Sci Total Environ 2017;610-611:1154–63.
[18] Ren X, Zeng G, Tang L, Wang J, Wan J, Feng H. Effect of exogenous carbonaceous materials on the bioavailability of organic pollutants and their ecological risks. Soil Biol Biochem 2018;116:70–81.
[19] Zhou Y, Tang L, Zeng G, Zhang C, Zhang Y, Xie X. Current progress in biosensors for heavy metal ions based on DNAzymes/DNA molecules functionalized nanostructures: a review. Sensor Actuat B Chem 2016;223:280–94.
[20] Wang P, Tang L, Wei X, Zeng G, Zhou Y, Deng Y. Synthesis and application of iron and zinc doped biochar for removal of p -nitrophenol in wastewater and assessment of the influence of co-existed Pb(II). Appl Surf Sci 2016;392:391–401.
[21] Tang L, Yang GD, Zeng GM, Cai Y, Li SS, Zhou YY. Synergistic effect of iron doped ordered mesoporous carbon on adsorption-coupled reduction of hexavalent chromium and the relative mechanism study. Chem Eng J 2014;239:114–22.
[22] Lee H, Yanilmaz M, Toprakci O, Fu K, Zhang X. A review of recent developments in membrane separators for rechargeable lithium-ion batteries. Energ Environ Sci 2014;7:3857–86.
[23] Lu X, Yu M, Wang G, Tong Y, Li Y. Flexible solid-state supercapacitors: design, fabrication and applications. Energ Environ Sci 2014;7:2160–81.
[24] Yu Z, Tetard L, Zhai L, Thomas J. Supercapacitor electrode materials: nanostructures from 0 to 3 dimensions. Energ Environ Sci 2015;8:702–30.
[25] Jiang H, Lee PS, Li C. 3D carbon based nanostructures for advanced supercapacitors. Energ Environ Sci 2012;6:41–53.
[26] Yan J, Wang Q, Lin C, Wei T, Fan Z. Interconnected frameworks with a sandwiched porous carbon layer/graphene hybrids for supercapacitors with high gravimetric and volumetric performances. Adv Energ Mater 2015;4:1294–305.
[27] Guo X, Brault P, Zhi G, Caillard A, Jin G, Guo X. Structural evolution of plasma-sputtered core–shell nanoparticles for catalytic combustion of methane. J Phys Chem C 2011;115:24164–71.
[28] Zhu SJ, Li L, Liu JB, Wang HT, Wang T, Zhang YX. Structural directed growth of ultrathin parallel birnessite on β-MnO_2 for high-performance asymmetric supercapacitors. ACS Nano 2018;12:1033–42.
[29] Liu Y, Zhou B, Li J, Gan X, Jing B, Cai W. Preparation of short, robust and highly ordered TiO2 nanotube arrays and their applications as electrode. Appl Catal B Environ 2009;92:326–32.
[30] Wang H, Wu Y, Yuan X, Zeng G, Zhou J, Wang X. Clay-inspired MXene-based electrochemical devices and photo-electrocatalyst: state-of-the -art progresses and challenges. Adv Mater 2018;30:1704561.
[31] Feng JX, Wu JQ, Tong Y, Li GR. Efficient hydrogen evolution on Cu nanodots-decorated Ni_3S_2 nanotubes by optimizing atomic hydrogen adsorption and desorption. J Am Chem Soc 2018;140:610–7.
[32] Gawande MB, Bonifacio VDB, Luque R, Branco PS, Varma RS. ChemInform abstract: benign by design: catalyst-free in-water, on-water green chemical methodologies in organic synthesis. Chem Soc Rev 2013;44:5522–51.
[33] Gawande MB, Bonifácio VD, Luque R, Branco PS, Varma RS. Solvent-free and catalysts-free chemistry: a benign pathway to sustainability. Chemsuschem 2014;45:24–44.
[34] Wang H, Yan W, Mingbao F, Wenguang T, Tong X, Ting X. Visible-light-driven removal of tetracycline antibiotics and reclamation of hydrogen energy from natural water matrices and wastewater by polymeric carbon nitride foam. Water Res 2018;144:215–25.
[35] Wu Y, Wang H, Tu W, Liu Y, Wu S, Tan YZ. Construction of hierarchical 2D-2D $Zn_3In_2S_6$/fluorinated polymeric carbon nitride nanosheets photocatalyst for boosting photocatalytic degradation and hydrogen production performance. Appl Catal B Environ 2018;233:58–69.
[36] Zhang J, Wang H, Yuan X, Zeng G, Tu W, Wang S. Tailored indium sulfide-based materials for solar-energy conversion and utilization. J Photoch Photobio 2019;38:1–26.
[37] Lauhon LJ, Gudiksen MS, Wang D, Lieber CM. Epitaxial core@shell and core@multishell nanowire heterostructures. Nature 2002;420:57–61.
[38] Pang X, Zhao L, Han W, Xin X, Lin Z. A general and robust strategy for the synthesis of nearly monodisperse colloidal nanocrystals. Nat Nanotechnol 2013;8:426.
[39] Jiang HL, Akita T, Ishida T, Haruta M, Xu Q. Synergistic catalysis of Au@Ag core-shell nanoparticles stabilized on metal-organic framework. J Am Chem Soc 2011;133:1304–6.
[40] Wang D, Li Y. Bimetallic nanocrystals: liquid–phase synthesis and catalytic applications. Adv Mater 2011;23:1044.
[41] Adijanto L, Bennett DA, Chen C, Yu AS, Cargnello M, Fornasiero P. Exceptional thermal stability of Pd@CeO_2 core-shell catalyst nanostructures grafted onto an oxide surface. Nano Lett 2013;13:2252.
[42] Cha W, Jeong NC, Song S, Park HJ, Thanh Pham TC, Harder R. Core-shell strain structure of zeolite microcrystals. Nat Mater 2013;12:729.
[43] Wang H, Wu Y, Xiao T, Yuan X, Zeng G, Tu W. Formation of quasi-core-shell In_2S_3/anatase TiO_2 @metallic $Ti_3C_2T_x$ hybrids with favorable charge transfer channels for excellent visible-light-photocatalytic performance. Appl Catal B Environ 2018;233:213–25.
[44] Wang D, Xin HL, Wang H, Yu Y, Rus E, Muller DA. Facile synthesis of carbon-supported Pd–Co core–shell nanoparticles as oxygen reduction electrocatalysts and their enhanced activity and stability with monolayer Pt decoration. Chem Mater 2012;24(12):2274–81.
[45] Wei H, Wang J, Li Z, Yang S. Fabrication of Co_3O_4@Co–Ni sulfides core/shell nanowire arrays as binder-free electrode for electrochemical energy storage. Energy 2015;93:435–41.
[46] Xu Y, Ruban AV, Mavrikakis M. Adsorption and dissociation of O_2 on Pt-Co and Pt-Fe alloys. J Am Chem Soc 2004;126:4717–25.
[47] Hammer B, Nørskov JK. Theoretical surface science and catalysis-calculations and concepts. Adv Catal 2000;45:71–129.
[48] Du J, Qi J, Wang D, Tang Z. Facile synthesis of Au@TiO_2 core–shell hollow spheres for dye-sensitized solar cells with remarkably improved efficiency. Energ Environ Sci 2012;5:6914–8.
[49] Wang D, Li Y. One-pot protocol for Au-based hybrid magnetic nanostructures via a noble-metal-induced reduction process. J Am Chem Soc 2010;132:6280.
[50] Strasser P, Koh S, Anniyev T, Greeley J, More K, Yu C. Lattice-strain control of the activity in dealloyed core-shell fuel cell catalysts. Nat Chem 2010;2:454.
[51] Dong H, Wu Z, Lu F, Gao Y, El-Shafei A, Jiao B. Optics–electrics highways: plasmonic silver nanowires@TiO_2 core–shell nanocomposites for enhanced dye-sensitized solar cells performance. Nano Energy 2014;10:181–91.
[52] Liu M, Qian J, Zhao Y, Zhu D, Gan L, Chen L. Core–shell ultramicroporous@microporous carbon nanospheres as advanced supercapacitor electrodes. J Mater Chem A 2015;3:11517–26.
[53] Fedorov MV, Kornyshev AA. Ionic Liquids at Electrified Interfaces. Chem Rev 2014;114:2978–3036.
[54] Zhang J, Zhang X, Zhou Y, Guo S, Wang K, Liang Z. Nitrogen-doped hierarchical porous carbon nanowhisker ensembles on carbon nanofiber for high-performance supercapacitors. ACS Sustain Chem Eng 2014;2:1525–33.
[55] Ghosh CR, Paria S. Core/shell nanoparticles: classes, properties, synthesis mechanisms, characterization, and applications. Chem Rev 2012;112:2373–433.
[56] Zhou W, Cao X, Zeng Z, Shi W, Zhu Y, Yan Q. One-step synthesis of Ni_3S_2 nanorod@Ni$(OH)_2$ nanosheet core–shell nanostructures on a three-dimensional graphene network for high-performance supercapacitors. Energ Environ Sci 2013;6:2216–21.
[57] Yao Y, Ma C, Wang J, Qiao W, Ling L, Long D. Rational design of high-surface-area carbon nanotube/microporous carbon core-shell nanocomposites for supercapacitor electrodes. ACS Appl Mater Interf 2015;7:4817.
[58] Gong JL, Wang B, Zeng GM, Yang CP, Niu CG, Niu QY. Removal of cationic dyes from aqueous solution using magnetic multi-wall carbon nanotube nanocomposite as adsorbent. J Hazard Mater 2008;164:1517–22.
[59] Yang X, Zhang F, Zhang L, Zhang T, Huang Y, Chen Y. A high-performance graphene oxide-doped ion gel as gel polymer electrolyte for all-solid-state supercapacitor applications. Adv Funct Mater 2013;23:3353–60.
[60] Richey FW, Tran C, Kalra V, Elabd YA. Ionic liquid dynamics in nanoporous carbon nanofibers in supercapacitors measured with in operando infrared spectroelectrochemistry. J Phys Chem C 2014;118:21846–55.
[61] Qian X, Lv Y, Li W, Xia Y, Zhao D. Multiwall carbon nanotube@mesoporous carbon with core-shell configuration: a well-designed composite-structure toward electrochemical capacitor application. J Mater Chem 2011;21:13025.
[62] Qin Z, Taylor M, Hwang M, Bertoldi K, Buehler MJ. Effect of wrinkles on the surface area of graphene: toward the design of nanoelectronics. Nano Lett 2014;14:6520.
[63] Lin LY, Yeh MH, Tsai JT, Huang YH, Sun CL, Ho KC. A novel core–shell multi-walled carbon nanotube@graphene oxide nanoribbon heterostructure as a potential supercapacitor material. J Mater Chem A 2013;1:11237–45.
[64] Zhang X, Yan P, Zhang R, Jin J, Xu J, Wu C. Fabrication of graphene and core–shell activated porous carbon-coated carbon nanotube hybrids with excellent electrochemical performance for supercapacitors. Int J Hydrogen Energ 2016;41:6394–402.
[65] Frackowiak E. Carbon materials for supercapacitor application. Phys Chem Chem Phys 2007;9:1774–85.
[66] Vol'Fkovich YM, Serdyuk TM. Electrochemical Capacitors. Russ J Electrochem 2002;38:935–59.
[67] Warren CR, Tausz M, Adams MA. Electrochemical modification of active carbon fiber electrode and its application to double-layer capacitor. J Power Sources 1996;60:249–53.
[68] Béguin F, Szostak K, Lota G, Frackowiak E. A self-supporting electrode for supercapacitors prepared by one-step pyrolysis of carbon nanotube/polyacrylonitrile blends. Adv Mater 2005;17:2380–4.

[69] Hulicova D, Yamashita J, Soneda Y, Hiroaki Hatori A, Kodama M. Supercapacitors prepared from melamine-based carbon. Chem Mater 2005;17:1241–7.
[70] Hulicova D, Masaya Kodama A, Hatori H. Electrochemical performance of nitrogen-enriched carbons in aqueous and non-aqueous supercapacitors. Chem Mater 2006; 18:2318–26.
[71] Lota G, Grzyb B, Machnikowska H, Machnikowski J, Frackowiak E. Effect of nitrogen in carbon electrode on the supercapacitor performance. Chem Phys Lett 2005;404: 53–8.
[72] Seredych M, Hulicova-Jurcakova D, Gao QL, Bandosz TJ. Surface functional groups of carbons and the effects of their chemical character, density and accessibility to ions on electrochemical performance. Carbon 2008;46:1475–88.
[73] Yang G, Lin Tang, Zeng G, Ye C, Tang J, Pang Y. Simultaneous removal of lead and phenol contamination from water by nitrogen-functionalized magnetic ordered mesoporous carbon. Chem Eng J 2015;259:854–64.
[74] Wu Z, Zhong H, Yuan X, Wang H, Wang L, Chen X. Adsorptive removal of methylene blue by rhamnolipid-functionalized graphene oxide from wastewater. Water Res 2014;67:330–44.
[75] Leng L, Yuan X, Zeng G, Shao J, Chen X, Wu Z. Surface characterization of rice husk bio-char produced by liquefaction and application for cationic dye (Malachite green) adsorption. Fuel 2015;155:77–85.
[76] Zhang Y, Feng H, Wu X, Wang L, Zhang A, Xia T. Progress of electrochemical capacitor electrode materials: A review. Int J Hydrogen Energ 2009;34:4889–99.
[77] Qu D. Studies of the activated carbons used in double-layer supercapacitors. J Power Sources 2002;109:403–11.
[78] Liu B, Liu B, Wang Q, Wang X, Xiang Q, Chen D. New energy storage option: toward $ZnCo_2O_4$ nanorods/nickel foam architectures for high-performance supercapacitors. ACS Appl Mater Interf 2013;5:10011–7.
[79] Shang C, Dong S, Wang S, Xiao D, Han P, Wang X. Coaxial $NixCo_{2x}(OH)_{6x}$/TiN nanotube arrays as supercapacitor electrodes. ACS Nano 2013;7:5430–6.
[80] Zhang J, Fu J, Zhang J, Ma H, He Y, Li F. Co@Co_3O_4 core-shell three-dimensional nano-network for high-performance electrochemical energy storage. Small 2014; 10:2618–24.
[81] Kalaji M, Murphy PJ, Williams GO. The study of conducting polymers for use as redox supercapacitors. Synthetic Met 1999;102:1360–1.
[82] Zhou YK, He BL, Zhou WJ, Huang J, Li XH, Wu B. Electrochemical capacitance of well-coated single-walled carbon nanotube with polyaniline composites. Electrochim Acta 2004;49:257–62.
[83] Gupta V, Miura N. High performance electrochemical supercapacitor from electrochemically synthesized nanostructured polyaniline. Mater Lett 2006;60:1466–9.
[84] Fan LZ, Maier J. Composite effects in poly(ethylene oxide)–succinonitrile based all-solid electrolytes. Electrochem Commun 2006;8:1753–6.
[85] Lin T, Fang Y, Pang Y, Zeng G, Wang J, Zhou Y. Synergistic adsorption and reduction of hexavalent chromium using highly uniform polyaniline–magnetic mesoporous silica composite. Chem Eng J 2014;254:302–12.
[86] Jabeen N, Xia Q, Mei Y, Hui X. Unique core–shell nanorod arrays with polyaniline deposited into mesoporous $NiCo_2O_4$ support for high-performance supercapacitor electrodes. ACS Appl Mater Interf 2016;8:6093.
[87] Ma W, Shi Q, Nan H, Hu Q, Zheng X, Geng B. Hierarchical ZnO@MnO_2@PPy ternary core-shell nanorod arrays: an efficient integration of active materials for energy storage. RSC Adv 2015;5:39864–9.
[88] Lota K, Khomenko V, Frackowiak E. Capacitance properties of poly(3,4-ethylenedioxythiophene)/carbon nanotubes composites. J Phys Chem Solid 2004; 65:295–301.
[89] Li W, Chen J, Zhao J, Zhang J, Zhu J. Application of ultrasonic irradiation in preparing conducting polymer as active materials for supercapacitor. Mater Lett 2005;59: 800–3.
[90] Hu X, Xiong W, Wang W, Qin S, Cheng H, Zeng Y. Hierarchical manganese dioxide/poly(3,4-ethylenedioxythiophene) core–shell nanoflakes on ramie-derived carbon fiber for high-performance flexible all-solid-state supercapacitor. ACS Sustain Chem Eng 2016;4:3.
[91] Li X, Shen J, Sun W, Wang RT, Hong X, Zhao X. A super-high energy density asymmetric supercapacitor based on 3D core–shell structured NiCo-layered double hydroxide@carbon nanotube and activated polyaniline-derived carbon electrodes with commercial level mass loading. J Mater Chem A 2015; 3:13244–53.
[92] Wang X, Xiao Y, Su D, Zhou L, Wu S, Han L. High-quality porous cobalt monoxide nanowires @ ultrathin manganese dioxide sheets core-shell nanowire arrays on Ni foam for high-performance supercapacitor. Electrochim Acta 2016;194:377–84.
[93] Zhao DD, Bao SJ, Zhou WJ, Li HL. Preparation of hexagonal nanoporous nickel hydroxide film and its application for electrochemical capacitor. Electrochem Commun 2007;9:869–74.
[94] Bouroushian M, Karoussos D, Kosanovic TBE. Conway, Electrochemical Supercapacitors: Scientific Fundamentals and Technological Applications. New York: Kluwer Academic/Plenum Publisher; 1999; 2006.
[95] Han L, Tang P, Zhang L. Hierarchical Co_3O_4 @PPy@MnO_2 core–shell–shell nanowire arrays for enhanced electrochemical energy storage. Nano Energy 2014;7:42–51.
[96] Zhang Z, Ma C, He L, Huang M, Yu L, Zhang Y. Facile synthesis of ATO/MnO_2 core–shell architectures for electrochemical capacitive energy storage. Ceram Int 2014; 40:10309–15.
[97] Jiang H, Li C, Sun T, Ma J. High-performance supercapacitor material based on Ni$(OH)_2$ nanowire-MnO_2 nanoflakes core-shell nanostructures. Chem Commun 2012;48:2606–8.
[98] Chang JK, Huang CH, Lee MT, Tsai WT, Deng MJ, Sun IW. Physicochemical factors that affect the pseudocapacitance and cyclic stability of Mn oxide electrodes. Electrochim Acta 2009;54:3278–84.
[99] Liu D, Wang Q, Qiao L, Li F, Wang D, Yang Z. Preparation of nano-networks of MnO_2 shell/Ni current collector core for high-performance supercapacitor electrodes. J Mater Chem 2011;22:483–7.
[100] Ming H, Fei L, Xiao LZ, Da L, Xue QY, Yu XZ. Hierarchical ZnO@MnO_2 core-shell pillar arrays on Ni foam for binder-free supercapacitor electrodes. Electrochim Acta 2014;152:172–7.
[101] Qiu K, Lu Y, Zhang D, Cheng J, Yan H, Xu J. Mesoporous, hierarchical core/shell structured $ZnCo_2O_4$/MnO_2 nanocone forests for high-performance supercapacitors. Nano Energy 2015;11:687–96.
[102] Wang HY, Xiao FX, Yu L, Liu B, Lou XW. Hierarchical α–MnO_2 Nanowires@Ni_{1-x}MnxOy nanoflakes core@shell nanostructures for supercapacitors. Small 2014; 10:3181–6.
[103] Wang K, Shi Z, Wang Y, Ye Z, Xia H, Liu G. Co_3O_4 nanowires@MnO_2 nanolayer or nanoflakes core–shell arrays for high-performance supercapacitors: The influence of morphology on performance. J Alloys Compd 2015;624:85–93.
[104] Nam KW, Kim KH, Lee ES, Yoon WS, Yang XQ, Kim KB. Pseudocapacitive properties of electrochemically prepared nickel oxides on 3-dimensional carbon nanotube film substrates. J Power Sources 2008;182:642–52.
[105] Li Y, Peng H, Zhang C, Chu M, Xiao P, Zhang Y. Branched ultra-fine nickel oxide/manganese dioxide core-shell nanosheet arrays for electrochemical capacitor. RSC Adv 2015;5:77115–21.
[106] Han D, Xu P, Jing X, Wang J, Song D, Liu J. Facile approach to prepare hollow core–shell NiO microspherers for supercapacitor electrodes. J Solid State Chem 2013; 203:60–7.
[107] Chen H, Qi XQ, Kuang M, Dong F, Zhang YX. Hierarchical copper/nickel-based manganese dioxide core-shell nanostructure for supercapacitor electrodes. Electrochim Acta 2016;212:671–7.
[108] Li Q, Liang CL, Lu XF, Tong YX, Li GR. Ni@NiO core–shell nanoparticle tube arrays with enhanced supercapacitor performance. J Mater Chem A 2015;3:6432–9.
[109] Wu JB, Guo RQ, Huang XH, Lin Y. Construction of self-supported porous TiO_2/NiO core/shell nanorod arrays for electrochemical capacitor application. J Power Sources 2013;243:317–22.
[110] Huang M, Li F, Zhang YX, Li B, Gao X. Hierarchical NiO nanoflake coated CuO flower core–shell nanostructures for supercapacitor. Ceram Int 2014;40:5533–8.
[111] Hu Y, Tolmachev YV, Scherson DA. Rotating ring-disk studies of oxidized nickel hydrous oxide: oxygen evolution and pseudocapacitance. J Electroanal Chem 1999; 468:64–9.
[112] Yin X, Tang C, Zhang L, Yu ZG, Gong H. Chemical insights into the roles of nanowire cores on the growth and supercapacitor performances of Ni-Co-O/Ni$(OH)_2$ core/shell electrodes. Sci Rep 2016;6:21566.
[113] Li N, Wang JY, Liu ZQ, Guo YP, Wang DY, Su YZ. One-dimensional ZnO/Mn_3O_4 core/shell nanorod and nanotube arrays with high supercapacitive performance for electrochemical energy storage. RSC Adv 2014;4:17274–81.
[114] Li GR, Wang ZL, Zheng FL, Ou YN, Tong YX. ZnO@MoO_3 core/shell nanocables: facile electrochemical synthesis and enhanced supercapacitor performances. J Mater Chem 2011;21:4217–21.
[115] Li Z, Shao M, Zhou L, Zhang R, Zhang C, Han J. A flexible all-solid-state micro-supercapacitor based on hierarchical CuO@layered double hydroxide core–shell nanoarrays. Nano Energy 2016;20:294–304.
[116] Li R, Ren X, Zhang F, Du C, Liu J. Synthesis of Fe_3O_4@SnO_2 core-shell nanorod film and its application as a thin-film supercapacitor electrode. Chem Commun 2012; 48:5010.
[117] Lee H, Hong S, Lee J, Suh YD, Kwon J, Moon H. Highly stretchable and transparent supercapacitor by Ag-Au core-shell nanowire network with high electrochemical stability. ACS Appl Mater Interf 2016;8:15449–58.
[118] Yuksel R, Coskun S, Unalan HE. Coaxial silver nanowire network core molybdenum oxide shell supercapacitor electrodes. Electrochim Acta 2016;193:39–44.
[119] Izadi-Najafabadi A, Yasuda S, Kobashi K, Yamada T, Futaba DN, Hatori H. Extracting the full potential of single-walled carbon nanotubes as durable supercapacitor electrodes operable at 4 V with high power and energy density. Adv Mater 2010;22: 235–41.
[120] Chen PC, Shen G, Shi Y, Chen H, Zhou C. Preparation and characterization of flexible asymmetric supercapacitors based on transition-metal-oxide nanowire/single-walled carbon nanotube hybrid thin-film electrodes. ACS Nano 2010;4: 4403–11.
[121] Wu ZS, Ren W, Wang DW, Li F, Liu B, Cheng HM. High-energy MnO_2 nanowire/graphene and graphene asymmetric electrochemical capacitors. ACS Nano 2010; 4:5835–42.
[122] Cericola D, Ruch PW, Kötz R, Novák P, Wokaun A. Characterization of bi-material electrodes for electrochemical hybrid energy storage devices. Electrochem Commun 2010;12:812–5.
[123] Wang HQ, Li ZS, Huang YG, Li QY, Wang XY. A novel hybrid supercapacitor based on spherical activated carbon and spherical MnO_2 in a non-aqueous electrolyte. J Mater Chem 2010;20:3883–9.
[124] Khomenko V, Raymundo-Piñero E, Béguin F. High-energy density graphite/AC capacitor in organic electrolyte. J Power Sources 2008;177:643–51.
[125] Wen Z, Wang Q, Zhang Q, Li J. In situ growth of mesoporous SnO_2 on multiwalled carbon nanotubes: a novel composite with porous–tube structure as anode for lithium batteries. Adv Funct Mater 2007;17:2772–8.
[126] Mohamed SG, Chen CJ, Chen CK, Hu SF, Liu RS. High-performance lithium-ion battery and symmetric supercapacitors based on $FeCo_2O_4$ nanoflakes electrodes. ACS Appl Mater Interf 2014;6:22701.
[127] Raymundo-Piñero E, Leroux F, Béguin F. A high–performance carbon for supercapacitors obtained by carbonization of a seaweed biopolymer. Adv Mater 2010;18:1877–82.

[128] Wei TY, Chen CH, Chang KH, Lu SY, Hu CC. Cobalt oxide aerogels of ideal supercapacitive properties prepared with an epoxide synthetic route. Chem Mater 2009;21:3228–33.
[129] Zhang H, Chen Y, Wang W, Zhang G, Zhuo M, Zhang H. Hierarchical Mo-decorated CoO nanowire arrays on Ni foam substrates for advanced electrochemical capacitors. J Mater Chem A 2013;1:8593–600.
[130] He Y, Chen W, Li X, Zhang Z, Fu J, Zhao C. Freestanding three-dimensional graphene/MnO_2 composite networks as ultralight and flexible supercapacitor electrodes. ACS Nano 2013;7:174–82.
[131] Xie Q, Bao R, Xie C, Zheng A, Wu S, Zhang Y. Core-shell N-doped active carbon fiber@graphene composites for aqueous symmetric supercapacitors with high-energy and high-power density. J Power Sources 2016;317:133–42.
[132] Wang Y, Yu Y, Li G, Liu L, Zhang H, Wang G. Sea urchin-like core/shell hierarchical porous carbon for supercapacitors. J Alloys Compd 2017;719:438–45.
[133] Lin L-Y, Yeh M-H, Tsai J-T, Huang Y-H, Sun C-L, Ho K-C. A novel core–shell multi-walled carbon nanotube@graphene oxide nanoribbon heterostructure as a potential supercapacitor material. J Mater Chem A 2013;1:11237.
[134] Wang J, Zhang X, Wei Q, Lv H, Tian Y, Tong Z. 3D self-supported nanopine forest-like Co_3O_4@$CoMoO_4$ core–shell architectures for high-energy solid state supercapacitors. Nano Energy 2016;19:222–33.
[135] Yuksel R, Coskun S, Kalay YE, Unalan HE. Flexible, silver nanowire network nickel hydroxide core-shell electrodes for supercapacitors. J Power Sources 2016;328:167–73.
[136] Zhang D, Zhang Y, Luo Y, Chu PK. Highly porous honeycomb manganese oxide@carbon fibers core–shell nanocables for flexible supercapacitors. Nano Energy 2015;13:47–57.
[137] Zhao B, Huang S-Y, Wang T, Zhang K, Yuen MMF, Xu J-B. Hollow SnO_2@Co_3O_4 core–shell spheres encapsulated in three-dimensional graphene foams for high performance supercapacitors and lithium-ion batteries. J Power Sources 2015;298:83–91.
[138] Gu Z, Zhang X. $NiCo_2O_4$@$MnMoO_4$core–shell flowers for high performance supercapacitors. J Mater Chem A 2016;4:8249–54.
[139] Sun J, Li W, Zhang B, Li G, Jiang L, Chen Z. 3D core/shell hierarchies of MnOOH ultrathin nanosheets grown on NiO nanosheet arrays for high-performance supercapacitors. Nano Energy 2014;4:56–64.
[140] Deng M-J, Ho P-J, Song C-Z, Chen S-A, Lee J-F, Chen J-M. Fabrication of Mn/Mn oxide core–shell electrodes with three-dimensionally ordered macroporous structures for high-capacitance supercapacitors. Energ Environ Sci 2013;6:2178.
[141] Li R, Wang S, Huang Z, Lu F, He T. $NiCo_2S_4$@$Co(OH)_2$ core-shell nanotube arrays in situ grown on Ni foam for high performances asymmetric supercapacitors. J Power Sources 2016;312:156–64.
[142] He W, Wang C, Zhuge F, Deng X, Xu X, Zhai T. Flexible and high energy density asymmetrical supercapacitors based on core/shell conducting polymer nanowires/manganese dioxide nanoflakes. Nano Energy 2017;35:242–50.
[143] Radhamani AV, Shareef KM, Rao MS. ZnO@MnO_2 core-shell nanofiber cathodes for high performance asymmetric supercapacitors. ACS Appl Mater Interf 2016;8:30531–42.
[144] Lu XF, Chen XY, Zhou W, Tong YX, Li GR. alpha-Fe_2O_3@PANI core-shell nanowire arrays as negative electrodes for asymmetric supercapacitors. ACS Appl Mater Interf 2015;7:14843–50.
[145] Tang X, Jia R, Zhai T, Xia H. Hierarchical Fe(3)O(4)@Fe(2)O(3) core-shell nanorod arrays as high-performance anodes for asymmetric supercapacitors. ACS Appl Mater Interf 2015;7:27518–25.
[146] Wang X, Xia H, Gao J, Shi B, Fang Y, Shao M. Enhanced cycle performance of ultraflexible asymmetric supercapacitors based on a hierarchical MnO_2@$NiMoO_4$core–shell nanostructure and porous carbon. J Mater Chem A 2016;4:18181–7.
[147] Kong W, Lu C, Zhang W, Pu J, Wang Z. Homogeneous core–shell $NiCo_2S_4$ nanostructures supported on nickel foam for supercapacitors. J Mater Chem A 2015;3:12452–60.
[148] Su L, Jing Y, Zhou Z. Li ion battery materials with core-shell nanostructures. Nanoscale 2011;3:3967–83.
[149] Zhong Y, Wu Z, Li J, Xiang W, Guo X, Zhong BH. Synthesis of core–shell structured $LiFe_{0.5}Mn_{0.3}Co_{0.2}PO_4$@C with remarkable electrochemical performance as the cathode of a lithium–ion battery. Chemelectrochem 2015;2:896–902.
[150] Wang HQ, Zhang XH, Zheng FH. Surfactant effect on synthesis of core-shell $LiFePO_4$/C cathode materials for lithium-ion batteries. J Solid State Electr 2015;19:187–94.
[151] Rui XH, Li C, Chen CH. Synthesis and characterization of carbon-coated $Li_3V_2(PO_4)_3$ cathode materials with different carbon sources. Electrochim Acta 2009;54:3374–80.
[152] Liu Y, Zhang M, Li Y, Hu Y, Zhu M, Jin H. Nano-sized $LiFePO_4$/C composite with core-shell structure as cathode material for lithium ion battery. Electrochim Acta 2015;176:689–93.
[153] Xu G, Li F, Tao Z, Wei X, Liu Y, Li X. Monodispersed $LiFePO_4$@C core–shell nanostructures for a high power Li-ion battery cathode. J Power Sources 2014;246:696–702.
[154] Doan TNL, Bakenov Z, Taniguchi I. Preparation of carbon coated $LiMnPO_4$ powders by a combination of spray pyrolysis with dry ball-milling followed by heat treatment. Adv Powder Technol 2010;21:187–96.
[155] Oh SM, Oh SW, Yoon CS, Scrosati B, Amine K, Sun YK. High-performance carbon-$LiMnPO_4$ nanocomposite cathode for lithium batteries. Adv Funct Mater 2010;20:3260–5.
[156] Doan TNL, Taniguchi I. Cathode performance of $LiMnPO_4$/C nanocomposites prepared by a combination of spray pyrolysis and wet ball-milling followed by heat treatment. J Power Sources 2011;196:1399–408.
[157] Cheng G, Zuo P, Wang L, Shi W, Ma Y, Du C. High-performance carbon-coated $LiMnPO_4$ nanocomposites by facile two-step solid-state synthesis for lithium-ion battery. J Solid State Electr 2015;19:281–8.
[158] Duan W, Hu Z, Zhang K, Cheng F, Tao Z, Chen J. $Li_3V_2(PO_4)_3$@C core-shell nanocomposite as a superior cathode material for lithium-ion batteries. Nanoscale 2013;5:6485–90.
[159] Zhang L, Wang S, Cai D, Lian P, Zhu X, Yang W. $Li_3V_2(PO_4)_3$@C/graphene composite with improved cycling performance as cathode material for lithium-ion batteries. Electrochim Acta 2013;91:108–13.
[160] Mao WF, Fu YB, Zhao H, Ai G, Dai YL, Meng D. Rational design and facial synthesis of $Li_3V_2(PO_4)_3$@C nanocomposites using carbon with different dimensions for ultrahigh-rate lithium-ion batteries. ACS Appl Mater Interf 2015;7:12057–66.
[161] Li Y, Makita Y, Lin Z, Lin S, Nagaoka N, Yang X. Synthesis and characterization of lithium manganese oxides with core-shell Li4Mn5O12@Li2MnO3 structure as lithium battery electrode materials. Solid State Ion 2011;196:34–40.
[162] Myung Seungtaek, Izumi Kentarou, Komaba Shinichi, Sun Yangkook, Hitoshi Yashiro A, Kumagai N. Role of alumina coating on Li—Ni—Co—Mn—O particles as positive electrode material for lithium-ion batteries. Chem Mater 2005;17:3695–704.
[163] Fey GTK, Weng ZX, Chen JG, Lu CZ. Preformed boehmite nanoparticles as coating materials for long-cycling $LiCoO_2$. J Appl Electrochem 2004;34:715–22.
[164] Alcántara R, Ortiz G, Tirado JL, Stoyanova R, Zhecheva E, Ivanova S. Fe^{3+} and Ni^{3+} impurity distribution and electrochemical performance of $LiCoO_2$ electrode materials for lithium ion batteries. J Power Sources 2009;194:494–501.
[165] Szczech JR, Song J. Nanostructured silicon for high capacity lithium battery anodes. Energ Environ Sci 2010;4:56–72.
[166] Tao H, Fan LZ, Song WL, Wu M, He X, Qu X. Hollow core-shell structured Si/C nanocomposites as high-performance anode materials for lithium-ion batteries. Nanoscale 2014;6:3138–42.
[167] Du C, Chen M, Wang L, Yin G. Covalently-functionalizing synthesis of Si@C core–shell nanocomposites as high-capacity anode materials for lithium-ion batteries. J Mater Chem 2011;21:15692–7.
[168] Zhao G, Zhang L, Meng Y, Zhang N, Sun K. High storage performance of core–shell Si@C nanoparticles as lithium ion battery anodematerial. Mater Lett 2013;96:170–3.
[169] Kim JS, Pfleging W, Kohler R, Seifert HJ, Kim TY, Byun D. Three-dimensional silicon/carbon core–shell electrode as an anode material for lithium-ion batteries. J Power Sources 2015;279:13–20.
[170] Zhou XY, Tang JJ, Yang J, Xie J, Ma LL. Silicon@carbon hollow core–shell heterostructures novel anode materials for lithium ion batteries. Electrochim Acta 2013;87:663–8.
[171] Kim YS, Kim KW, Cho D, Hansen NS, Lee J, Joo YL. Silicon-rich carbon hybrid nanofibers from water-based spinning: the synergy between silicon and carbon for Li-ion battery anode application. ChemElectroChem 2014;1:220–6.
[172] Wang W, Wang Y, Gu L, Lu R, Qian H, Peng X. SiC@Si core–shell nanowires on carbon paper as a hybrid anode forlithium-ion batteries. J Power Sources 2015;293:492–7.
[173] Li S, Wang Z, Liu J, Yang LY, Yue G, Cheng L. Yolk–shell Sn@C eggette-like nanostructure: application in lithium-ion and sodium-ion batteries. ACS Appl Mater Interf 2016;8:19438.
[174] Wang D, Li X, Yang J, Wang J, Geng D, Li R. Hierarchical nanostructured core-shell Sn@C nanoparticles embedded in graphene nanosheets: spectroscopic view and their application in lithium ion batteries. Phys Chem Chem Phys 2013;15:3535–42.
[175] Lian P, Wang J, Cai D, Liu G, Wang Y, Wang H. Design and synthesis of porous nanosized Sn@C/graphene electrode material with 3D carbon network for high-performance lithium-ion batteries. J Alloys Compd 2014;604:188–95.
[176] Zhang N, Zhao Q, Han X, Yang J, Chen J. Pitaya-like Sn@C nanocomposites as high-rate and long-life anode for lithium-ion batteries. Nanoscale 2014;6:2827–32.
[177] He Y, Huang L, Li X, Xiao Y, Xu GL, Li JT. Facile synthesis of hollow Cu_2Sb@C core–shell nanoparticles as a superior anode material for lithium ion batteries. J Mater Chem 2011;21:18517–9.
[178] Wang J, Li W, Wang F, Xia Y, Asiri AM, Zhao D. Controllable synthesis of SnO_2@C yolk-shell nanospheres as a high-performance anode material for lithium ion batteries. Nanoscale 2014;6:3217–22.
[179] Zhou D, Song WL, Fan LZ. Hollow core-shell SnO_2/C fibers as highly stable anodes for lithium-ion batteries. ACS Appl Mater Interf 2015;7:21472–8.
[180] Huang Y, Jia D, Guo Z, Cho WI, Dong Z. Preparation and characterization of core–shell structure Fe_3O_4/C nanoparticles with unique stability and high electrochemical performance for lithium-ion battery anode material. Electrochim Acta 2011;56:9233–9.
[181] Li L, Wang T, Zhang L, Su Z, Wang C, Wang R. Selected-control synthesis of monodisperse Fe_3O_4@C core-shell spheres, chains, and rings as high-performance anode materials for lithium-ion batteries. Chem Eur J 2012;18:11417–22.
[182] Cao B, Li Hou B, Mo Y, Yin L, Chen Y. Synthesis of double-shell SnO_2@C hollow nanospheres as sulfur/sulfide cages for lithium-sulfur batteries. ACS Appl Mater Interf 2016;8:27795–802.
[183] Li Y, Zhu S, Liu Q, Gu J, Guo Z, Chen Z. Carbon-coated SnO_2@C with hierarchically porous structures and graphite layers inside for a high-performance lithium-ion battery. J Mater Chem 2012;22:2766–73.
[184] Liu J, Li W, Manthiram A. Dense core-shell structured SnO_2/C composites as high performance anodes for lithium ion batteries. Chem Commun 2010;46:1437–9.
[185] Chen Z, Qin Y, Amine K, Sun YK. Role of surface coating on cathode materials for lithium-ion batteries. J Mater Chem 2010;20:7606–12.
[186] Shen L, Li H, Uchaker E, Zhang X, Cao G. General strategy for designing core-shell nanostructured materials for high-power lithium ion batteries. Nano Lett 2012;12:5673–8.

[187] Yang J, Wang J, Tang Y, Wang D, Xiao B, Li X. In situ self-catalyzed formation of core–shell $LiFePO_4$@CNT nanowires for high rate performance lithium-ion batteries. J Mater Chem A 2013;1:7306–11.
[188] Wang G, Ma Z, Shao G, Kong L, Gao W. Synthesis of $LiFePO_4$@carbon nanotube core–shell nanowires with a high-energy efficient method for superior lithium ion battery cathodes. J Power Sources 2015;291:209–14.
[189] Pan F, Wang W-L. Synthesis and characterization of core–shell F-doped $LiFePO_4$/C composite for lithium-ion batteries. J Solid State Electr 2011;16:1423–7.
[190] Li H, Chen Y, Chen L, Jiang H, Wang Y, Wang H. Improved cycling and high rate performance of core-shell LiFe1/3Mn1/3Co1/3PO4/carbon nanocomposites for lithium-ion batteries: Effect of the carbon source. Electrochim Acta 2014;143:407–14.
[191] Hieu NT, Suk J, Kim DW, Park JS, Kang Y. Electrospun nanofibers with a core–shell structure of silicon nanoparticles and carbon nanotubes in carbon for use as lithium-ion battery anodes. J Mater Chem A 2014;2:15094.
[192] Source J, Bordes A, Boulineau A, Alper JP, Franger S, Quinsac A. Core-shell amorphous silicon-carbon nanoparticles for high performance anodes in lithium ion batteries. J Power Sources 2016;328:527–35.
[193] Wu J, Qin X, Miao C, He Y-B, Liang G, Zhou D. A honeycomb-cobweb inspired hierarchical core–shell structure design for electrospun silicon/carbon fibers as lithium-ion battery anodes. Carbon 2016;98:582–91.
[194] Cao X, Chuan X, Masse RC, Huang D, Li S, Cao G. A three layer design with mesoporous silica encapsulated by carbon core and shell for high energy Lithium ion battery anode. J Mater Chem A 2015;3:22739–49.
[195] Jeong G, Kim JG, Park MS, Seo M, Hwang SM, Kim YU. Core-shell structured silicon nanoparticles@TiO_{2-x}/carbon mesoporous microfiber composite as a safe and high-performance lithium-ion battery anode. ACS Nano 2014;8:2977.
[196] Ngo DT, Le HTT, Kalubarme RS, Lee JY, Park CN, Park CJ. Uniform GeO dispersed in nitrogen-doped porous carbon core–shell architecture: an anode material for lithium ion batteries. J Mater Chem A 2015;3:21722–32.
[197] Yuan C, Cao H, Zhu S, Hua H, Hou L. Core–shell ZnO/$ZnFe_2O_4$@C mesoporous nanospheres with enhanced lithium storage properties towards high-performance Li-ion batteries. J Mater Chem A 2015;3:20389–98.
[198] Zhang Z, Wang F, An Q, Li W, Wu P. Synthesis of graphene@Fe_3O_4@C core–shell nanosheets for high-performance lithium ion batteries. J Mater Chem A 2015;3:7036–43.
[199] Park S-H, Lee W-J. Hierarchically mesoporous flower-like cobalt oxide/carbon nanofiber composites with shell–core structure as anodes for lithium ion batteries. Carbon 2015;89:197–207.
[200] Wang S, Xing Y, Xiao C, Xu H, Zhang S. A peapod-inspired MnO@C core-shell design for lithium ion batteries. J Power Sources 2016;307:11–6.
[201] Liu H, Li Z, Liang Y, Fu R, Wu D. Facile synthesis of MnO multi-core@nitrogen-doped carbon shell nanoparticles for high performance lithium-ion battery anodes. Carbon 2015;84:419–25.
[202] Dillon AC, Jones KM, Bekkedahl TA, Kiang CH, Bethune DS, Heben MJ. Storage of hydrogen in single-walled carbon nanotubes. Nature 1997;386:377–9.
[203] Liu C, Yang QH, Tong Y, Cong HT, Cheng HM. Volumetric hydrogen storage in single-walled carbon nanotubes. Appl Phys Lett 2002;80:2389–91.
[204] Chambers A, Park C, Baker RTK, Rodriguez NM. Hydrogen storage in graphite nanofibers. J Phys Chem B 1998;102:4253–6.
[205] Ye Y, Ahn CC, Witham C, Fultz B, Liu J, Rinzler AG. Hydrogen adsorption and cohesive energy of single-walled carbon nanotubes. Appl Phys Lett 1999;74:2307–9.
[206] Zacharia R, Rather SU, Sang WH, Nahm KS. Spillover of physisorbed hydrogen from sputter-deposited arrays of platinum nanoparticles to multi-walled carbon nanotubes. Chem Phys Lett 2007;434:286–91.
[207] Cheng C, Gao P, Bao D, Wang L, Wang Y, Chen Y. Ball-milling preparation of one-dimensional Co–carbon nanotube and Co–carbon nanofiber core/shell nanocomposites with high electrochemical hydrogen storage ability. J Power Sources 2014;255:318–24.
[208] Bao D, Gao P, Shen X, Cheng C, Wang L, Wang Y. Mechanical ball-milling preparation of fullerene/cobalt core/shell nanocomposites with high electrochemical hydrogen storage ability. ACS Appl Mater Interf 2014;6:2902.
[209] Orimo Shinichi, Nakamori Yuko, JRE Andreas Züttel A, CMJ. Complex hydrides for hydrogen storage. Chem Rev 2007;107:4111.
[210] Serkov AA, Barmina EV, Simakin AV, Kuzmin PG, Voronov VV, Shafeev GA. Generation of core–shell nanoparticles Al@Ti by laser ablation in liquid for hydrogen storage. Appl Surf Sci 2015;348:71–4.
[211] Konda SK, Ostrom CK, Chen A. Synthesis and electrochemical study of Cd@Pd core/shell nanomaterials for hydrogen sorption and storage. Int J Hydrogen Energ 2015;40:16365–74.
[212] Christian ML, Agueyzinsou KF. Core–shell strategy leading to high reversible hydrogen storage capacity for $NaBH_4$. ACS Nano 2012;6:7739–51.
[213] Li Y, Fu ZY, Su BL. Hierarchically structured porous materials for energy conversion and storage. Adv Funct Mater 2012;22:4634–67.
[214] Li Y, Yang X, Feng Y, Yuan Z, Su B. One-dimensional metal oxide nanotubes, nanowires, nanoribbons, and nanorods: synthesis, characterizations, properties and applications. Crit Rev Solid State 2012;37:1–74.
[215] XC Mao. Titanium dioxide nanomaterials: synthesis, properties, modifications, and applications. Chem Rev 2007;107:2891.
[216] Mahmood K, Swain BS, Kirmani AR, Amassian A. Highly efficient perovskite solar cells based on a nanostructured WO –TiO core–shell electron transporting material. J Mater Chem A 2015;3:9051–7.
[217] Pang A, Sun X, Ruan H, Li Y, Dai S, Wei M. Highly efficient dye-sensitized solar cells composed of TiO_2@SnO_2 core–shell microspheres. Nano Energy 2014;5:82–90.
[218] Qi J, Dang X, Hammond PT, Belcher AM. Highly efficient plasmon-enhanced dye-sensitized solar cells through metal@oxide core–shell nanostructure. ACS Nano 2011;5:7108–16.
[219] Liu WL, Lin FC, Yang YC, Huang CH, Gwo S, Huang MH. The influence of shell thickness of Au@TiO_2 core-shell nanoparticles on the plasmonic enhancement effect in dye-sensitized solar cells. Nanoscale 2013;5:7953–62.
[220] Yeh MH, Lin LY, Chou CY, Lee CP, Chuang HM, Vittal R. Preparing core–shell structure of ZnO@TiO_2 nanowires through a simple dipping–rinse–hydrolyzation process as the photoanode for dye-sensitized solar cells. Nano Energy 2013;2:609–21.
[221] Chen X, Bai Z, Yan X, Yuan H, Zhang G, Lin P. Design of efficient dye-sensitized solar cells with patterned ZnO-ZnS core-shell nanowire array photoanodes. Nanoscale 2014;6:4691–7.
[222] Samsuri SAM, Rahman MYA, Umar AA, Salleh MM. Effect of ZnO growth time on the performance of dye-sensitized solar cell utilizing TiO_2–ZnO core–shell nanograss hetero-structure. Mater Lett 2015;160:1503640.
[223] Song L, Jiang Q, Du P, Yang Y, Xiong J, Cui C. Novel structure of TiO_2–ZnO core shell rice grain for photoanode of dye-sensitized solar cells. J Power Sources 2014;261:1–6.
[224] Bora T, Kyaw HH, Dutta J. Zinc oxide–zinc stannate core–shell nanorod arrays for CdS quantum dot sensitized solar cells. Electrochim Acta 2012;68:141–5.
[225] Speirs MJ, Balazs DM, Fang HH, Lai LH, Protesescu L, Kovalenko MV. Origin of the increased open circuit voltage in PbS-CdS core-shell quantum dot solar cells. J Mater Chem A 2014;3:1450–7.
[226] Seo G, Seo JW, Ryu SC, Yin WP, Ahn TK, Seok S. Enhancing the Performance of Sensitized Solar Cells with PbS/ $CH_3NH_3PbI_3$ Core/Shell Quantum Dots. J Phys Chem Lett 2014;5:2015–20.
[227] Sehgal P, Narula AK. Synthesis and characterization of quantum dot sensitized solar cell based on PMOT@ CdTe @TiO_2 core shell nano structures. Electrochim Acta 2015;158:49–55.
[228] Azpiroz JM, Infante I, Angelis FD. First-principles modeling of core/shell quantum dot sensitized solar cells. J Phys Chem C 2015;119:12739–48.
[229] Zhang X, Liu J, Zhang J, Vlachopoulos N, Johansson EM. ZnO@Ag_2S core-shell nanowire arrays for environmentally friendly solid-state quantum dot-sensitized solar cells with panchromatic light capture and enhanced electron collection. Phys Chem Chem Phys 2015;17:12786–95.
[230] Wang J, Moraseró I, Pan Z, Zhao K, Zhang H, Feng Y. Core/shell colloidal quantum dot exciplex states for the development of highly efficient quantum-dot-sensitized solar cells. J Am Chem Soc 2013;135:15913–22.
[231] Yang J, Wang J, Zhao K, Izuishi T, Li Y, Shen Q. CdSeTe/CdS type-I core/shell quantum dot sensitized solar cells with efficiency over 9%. J Phys Chem C 2015;119:28800–8.
[232] Shen H, Jiao X, Dan O, Li J, Hong L. Efficient electron injection in non-toxic silver sulfide (Ag_2S) sensitized solar cells. J Power Sources 2013;240:8–13.
[233] Xu J, Chen Z, Zapien JA, Lee CS, Zhang W. ChemInform abstract: surface engineering of ZnO nanostructures for semiconductor–sensitized solar cells. Adv Mater 2014;26:5337–67.
[234] Ruffo R, Hong SS, Chan CK, Huggins RA, Cui Y. Impedance analysis of silicon nanowire lithium ion battery anodes. J Phys Chem C 2009;113:11390–8.
[235] Hochbaum AI, Chen R, Delgado RD, Liang W, Garnett EC, Najarian M. Enhanced Thermoelectric Performance of Rough Silicon Nanowires. Nature 2015;451:163–7.
[236] Boukai AI, Bunimovich Y, Tahirkheli J, Yu JK, Iii WAG, Heath JR. Silicon nanowires as efficient thermoelectric materials. Nature 2008;451:168–71.
[237] Kayes BM, Atwater HA, Lewis NS, Kayes BM, Atwater HA, Lewis NS. Comparison of the device physics principles of planar and radial p-n junction nanorod solar cells. J Appl Phys 2005;97:114302–11.
[238] Tsakalakos L, Balch J, Fronheiser J, Korevaar BA, Sulima O, Rand J. Silicon nanowire solar cells. Appl Phys Lett 2007;91:692.
[239] Tian B, Zheng X, Kempa TJ, Fang Y, Yu N, Yu G. Coaxial silicon nanowires as solar cells and nanoelectronic power sources. Nature 2007;449:885–9.
[240] Adachi MM, Anantram MP, Karim KS. Core-shell silicon nanowire solar cells. Sci Rep 2013;3:1546.
[241] Baek SW, Shim JH, Ko YH, Park JS, Lee GS, Jalalah M. Low-cost and flexible ultra-thin silicon solar cell implemented with energy-down-shift via $Cd_{0.5}Zn_{0.5}S$/ZnS core/shell quantum dots. J Mater Chem A 2014;3:481–7.
[242] Li G, Zhu R, Yang Y. Polymer solar cells. Nat Photonics 2012;6:153–61.
[243] Liu Z, Li J, Yan F. Package-free flexible organic solar cells with graphene top electrodes. Adv Mater 2013;25:4296–301.
[244] He Z, Xiao B, Liu F, Wu H, Yang Y, Xiao S. Single-junction polymer solar cells with high efficiency and photovoltage. Nat Photonics 2015;9:174–9.
[245] Liu S, Jiang R, You P, Zhu X, Wang J, Yan F. Au/Ag core-shell nanocuboids for high-efficiency organic solar cells with broadband plasmonic enhancement. Energ Environ Sci 2016;9:898–905.
[246] Baek SW, Park G, Noh J, Cho C, Lee CH, Seo MK. Au@Ag core-shell nanocubes for efficient plasmonic light scattering effect in low bandgap organic solar cells. ACS Nano 2014;8:3302–12.
[247] Chen B, Zhang W, Zhou X, Huang X, Zhao X, Wang H. Surface plasmon enhancement of polymer solar cells by penetrating Au/SiO_2 core/shell nanoparticles into all organic layers. Nano Energy 2013;2:906–15.
[248] Cho CY, Baek S, Kim K, Moon JH. 3D bicontinuous SnO_2/TiO_2 core/shell structures for highly efficient organic dye-sensitized solar cell electrodes. RSC Adv 2016;6:74003–8.
[249] Tan F, Qu S, Wang L, Jiang Q, Zhang W, Wang Z. Core/shell-shaped CdSe/PbS nanotetrapods for efficient organic-inorganic hybrid solar cells. J Mater Chem A 2014;2:14502–10.
[250] Amiri O, Salavati-Niasari M, Farangi M. Enhancement of dye-sensitized solar cells performance by core shell Ag@organic (organic=2-nitroaniline, PVA, 4-choloroaniline and PVP): effects of shell type on photocurrent. Electrochim Acta 2015;153:90–6.

[251] Qi J, Dang X, Hammond PT, Belcher AM. Highly efficient plasmon-enhanced dye-sensitized solar cells through metal@oxide core-shell nanostructure. ACS Nano 2011;5:7108.
[252] Gao C, Li X, Lu B, Chen L, Wang Y, Teng F. A facile method to prepare SnO2 nanotubes for use in efficient SnO_2-TiO_2 core-shell dye-sensitized solar cells. Nanoscale 2012;4:3475–81.
[253] Lim CK, Wang Y, Zhang L. Facile formation of a hierarchical TiO_2-SnO_2;nanocomposite architecture for efficient dye-sensitized solar cells. RSC Adv 2016;6:25114–22.
[254] Feng J, Hong Y, Zhang J, Wang P, Hu Z, Wang Q. Novel core–shell TiO_2 microsphere scattering layer for dye-sensitized solar cells. J Mater Chem A 2014;2:1502–8.
[255] Yu X, Xu H, Xin L, Wang X, Liu Y, Zhou X. Synergistic assembly of nanoparticle aggregates and texture nanosheets into hierarchical TiO_2 core–shell structures for enhanced light harvesting in dye-sensitized solar cells. J Mater Chem A 2013;1:6175.
[256] Son S, Hwang SH, Kim C, Yun JY, Jang J. Designed synthesis of SiO_2/TiO_2 core/shell structure as light scattering material for highly efficient dye-sensitized solar cells. ACS Appl Mater Interf 2013;5:4815–20.
[257] Zhang ZM, Hu Y, Qin FY, Ding YT. DC sputtering assisted nano-branched core-shell TiO_2/ZnO electrodes for application in dye-sensitized solar cells. Appl Surf Sci 2016;376:10–5.
[258] Gangishetty MK, Lee KE, Scott RW, Kelly TL. Plasmonic enhancement of dye sensitized solar cells in the red-to-near -infrared region using triangular core-shell Ag@SiO_2 nanoparticles. ACS Appl Mater Interf 2013;5:11044–51.
[259] Zhao P, Zhu Y, Yang X, Jiang X, Shen J, Li C. Plasmon-enhanced efficient dye-sensitized solar cells using core–shell-structured β-NaYF4:Yb,Er@SiO_2@Au nanocomposites. J Mater Chem A 2014;2:16523–30.
[260] Brown MD, Suteewong T, Kumar RS, D'Innocenzo V, Petrozza A, Lee MM. Plasmonic dye-sensitized solar cells using core-shell metal-insulator nanoparticles. Nano Lett 2011;11:438–45.
[261] Gonfa BA, Kim MR, Zheng P, Cushing SK, Qiao Q, Wu N. Investigation of plasmonic effect in air-processed PbS/CdS core-shell quantum dot based solar cells. J Mater Chem A 2016;4.
[262] Gonfa BA, Kim MR, Delegan N, Tavares AC, Izquierdo R, Wu N. Towards high efficiency air-processed near-infrared responsive photovoltaics: bulk heterojunction solar cells based on PbS/CdS core-shell quantum dots and TiO_2 nanorod arrays. Nanoscale 2015;7:10039–49.
[263] Song X, Wang M, Deng J, Ju Y, Xing T, Ding J. ZnO/PbS core/shell nanorod arrays as efficient counter electrode for quantum dot-sensitized solar cells. J Power Sources 2014;269:661–70.
[264] Tavakoli MM, Aashuri H, Simchi A, Kalytchuk S, Fan Z. Quasi core/shell lead sulfide/graphene quantum dots for bulk heterojunction solar cells. J Phys Chem C 2015;119:18886–95.
[265] Ahmed R, Zhao L, Mozer AJ, Will G, Bell J, Wang HX. Enhanced Electron Lifetime of CdSe/CdS Quantum Dot (QD) Sensitized Solar Cells Using ZnSe Core-Shell Structure with Efficient Regeneration of Quantum Dots. J Phys Chem C 2015;119:2297–307.
[266] Jiao S, Shen Q, Morasero I, Wang J, Pan Z, Zhao K. Band engineering in core/shell ZnTe/CdSe for photovoltage and efficiency enhancement in exciplex quantum dot sensitized solar cells. ACS Nano 2015;9:908–15.
[267] Baek SW, Shim JH, Park JG. The energy-down-shift effect of $Cd_{0.5}Zn_{0.5}$S-ZnS core-shell quantum dots on power-conversion-efficiency enhancement in silicon solar cells, Phys. Chem Chem Phys 2014;16:18205–10.
[268] Jia G, Eisenhawer B, Dellith J, Falk F, Thøgersen A, Ulyashin A. Multiple core–shell silicon nanowire-based heterojunction solar cells. J Phys Chem C 2013;117:1091–6.
[269] Togonal AS, Foldyna M, Chen W, Wang JX, Neplokh V, Tchernycheva M. Core–shell heterojunction solar cells based on disordered silicon nanowire arrays. J Phys Chem C 2016;120:2962–72.
[270] Baek SW, Park G, Noh J, Cho C, Lee CH, Seo MK. Au@Ag core-shell nanocubes for efficient plasmonic light scattering effect in low bandgap organic solar cells. ACS Nano 2014;8:3302–12.
[271] Baek SW, Park G, Noh JH, Cho CS, Lee CH, Seo MK, Song HJ, Lee JY. Au@Ag Core–Shell Nanocubes for Efficient Plasmonic Light Scattering Effect in Low Bandgap Organic Solar Cells. ACS Nano 2014;8:3302–12.
[272] Li Q, Yuan Y, Chen Z, Jin X, Wei TH, Li Y. Core-shell nanophosphor architecture: toward efficient energy transport in inorganic/organic hybrid solar cells. ACS Appl Mater Interf 2014;6:12798–807.
[273] Choi H, Song JH, Jang J, Mai XD, Kim S, Jeong S. High performance of PbSe/PbS core/shell quantum dot heterojunction solar cells: short circuit current enhancement without the loss of open circuit voltage by shell thickness control. Nanoscale 2015;7:17473–81.
[274] Hong Z, Xingwang LI, Wang F. Synthesis and characterization of Cu@Pt/C core-shell structured catalysts for proton exchange membrane fuel cell. Int.l J. Hydrogen Energ 2011;36:9151–4.
[275] Gan L, Heggen Marc, Rudi Stefan, Strasser. Core-shell compositional fine structures of dealloyed Pt_xNi_{1-x} nanoparticles and their impact on oxygen reduction catalysis. Nano Lett 2012;12:5423–30.
[276] Zhang C, Zhu A, Rong H, Zhang Q, Liu Q. Hollow nanoporous Au/Pt core–shell catalysts with nanochannels and enhanced activities towards electro-oxidation of methanol and ethanol. Int J Hydrogen Energ 2014;39:8246–56.
[277] Wang L, Yamauchi Y. Controlled aqueous solution synthesis of platinum-palladium alloy nanodendrites with various compositions using amphiphilic triblock copolymers. Chem Asian J 2010;5:2493–8.
[278] Hamed AE, Yoshihiro N, Masataka I, Yusuke Y. Facile synthesis of nanoporous Pt-Ru alloy spheres with various compositions toward highly active electrocatalysts. Chem Asian J 2012;7:876–80.
[279] Chai GS, Yoon SB, Kim JH, Yu JS. Spherical carbon capsules with hollow macroporous core and mesoporous shell structures as a highly efficient catalyst support in the direct methanol fuel cell. Chem Commun 2004;23:2766–7.
[280] Lin R, Cao C, Zhao T, Huang Z, Li B, Wieckowski A. Synthesis and application of core–shell Co@Pt/C electrocatalysts for proton exchange membrane fuel cells. J Power Sources 2013;223:190–8.
[281] Wang H, Wang L, Sato T, Sakamoto Y, Tominaka S, Miyasaka K. Synthesis of Mesoporous Pt Films with Tunable Pore Sizes from Aqueous Surfactant Solutions. Chem Mater 2012;24:1591–8.
[282] Li C, Takaaki S, Yusuke Y. Electrochemical synthesis of one-dimensional mesoporous Pt nanorods using the assembly of surfactant micelles in confined space. Angew Chem 2013;52:8050.
[283] Mahmoud MA, El-Sayed MA. Metallic double shell hollow nanocages: the challenges of their synthetic techniques. Langmuir 2012;28:4051–9.
[284] Liu CW, Wei YC, Liu CC, Wang KW. Pt–Au core/shell nanorods: preparation and applications as electrocatalysts for fuel cells. J Mater Chem 2012;22:4641–4.
[285] Rashid M, Jun T, Jung Y, Kim YS. Bimetallic core–shell Ag@Pt nanoparticle-decorated MWNT electrodes for amperometric H_2 sensors and direct methanol fuel cells. Sensor Actuat B Chem 2015;208:7–13.
[286] Du C, Chen M, Wang W, Tan Q, Xiong K, Yin G. Platinum-based intermetallic nanotubes with a core–shell structure as highly active and durable catalysts for fuel cell applications. J Power Sources 2013;240:630–5.
[287] Yang G, Dong C, Lv P, Kong X, Sun Y, Wang Z. Core-shell Au-Pd nanoparticles as cathode catalysts for microbial fuel cell applications. Sci Rep 2016;6:35252.
[288] Zhong S, Zhou L, Wu L, Tang L, He Q, Ahmed J. Nitrogen- and boron-co-doped core–shell carbon nanoparticles as efficient metal-free catalysts for oxygen reduction reactions in microbial fuel cells. J Power Sources 2014;272:344–50.
[289] Zhang J, Zhang X, Liu W, Liu H, Qiu J, Yeung KL. A new alkali-resistant Ni/Al_2O_3-MSU-1 core–shell catalyst for methane steam reforming in a direct internal reforming molten carbonate fuel cell. J Power Sources 2014;246:74–83.
[290] Lim CH, Lee KT. Characterization of core-shell structured Ni@GDC anode materials synthesized by ultrasonic spray pyrolysis for solid oxide fuel cells. Ceram Int 2016;42:13715–22.
[291] Lee MJ, Hong SK, Choi BH, Hwang HJ. Fabrication and performance of solid oxide fuel cell anodes from core–shell structured Ni/yttria-stabilized zirconia (YSZ) powders. Ceram Int 2016;42:10110–5.
[292] Wu J, Zhu B, Mi Y, Shih SJ, Wei J, Huang Y. A novel core–shell nanocomposite electrolyte for low temperature fuel cells. J Power Sources 2012;201:164–8.
[293] Lee J, Kim J, Hyeon T. Recent progress in the synthesis of porous carbon materials. Adv Mater 2011;18:2073–94.
[294] Vantomme A, Léonard A, Yuan ZY, Su BL. Self-formation of hierarchical micro-meso-macroporous structures: Generation of the new concept "hierarchical catalysis". Colloid Surf A 2007;300:70–8.
[295] Li F, Wang Z, Stein A. Shaping Mesoporous Silica Nanoparticles by Disassembly of Hierarchically Porous Structures. Angew Chem Ed Int 2007;46:1885–8.
[296] Wang X, Yu JC, Ho C, Hou Y, Fu X. Photocatalytic activity of a hierarchically macro/mesoporous titania. Langmuir 2005;21:2552–9.
[297] Yuan ZY, Ren TZ, Azioune A, Pireaux JJ, Su BL. Marvelous self-assembly of hierarchically nanostructured porous zirconium phosphate solid acids with high thermal stability. Catal Today 2005;105:647–54.
[298] Sun Z, Lv B, Li J, Xiao M, Wang XY, Du P. Core-shell amorphous cobalt phosphide/cadmium sulfide semiconductor nanorods for exceptional photocatalytic hydrogen production under visible light. J Mater Chem A 2016;4:1598–602.
[299] Wang C, Wang L, Jin J, Liu J, Li Y, Wu M. Probing effective photocorrosion inhibition and highly improved photocatalytic hydrogen production on monodisperse PANI@CdS core-shell nanospheres. Appl Catal B Environ 2016;188:351–9.
[300] Yang G, Yan W, Zhang Q, Shen S, Ding S. One-dimensional CdS/ZnO core/shell nanofibers via single-spinneret electrospinning: tunable morphology and efficient photocatalytic hydrogen production. Nanoscale 2013;5:12432–9.
[301] Kim HS, Kim D, Kwak BS, Han GB, Um M, Kang M. Synthesis of magnetically separable core@shell structured $NiFe_2O_4$@TiO_2 nanomaterial and its use for photocatalytic hydrogen production by methanol/water splitting. Chem Eng J 2014;243:272–9.